Trabajo Fin de Grado

Ingeniería Aeroespacial

Análisis numérico en DEFORM-3D de deformaciones límite en conformado incremental mono-punto de chapas de acero AISI304-H111

Numerical Analysis on DEFORM-3D of limit strains in Single Point Incremental Forming for AISI304-H111 sheets

Autor: Álvaro Fernández Díaz

Tutor: Gabriel Centeno Báez

Departamento de Ingeniería Mecánica y Fabricación
Escuela Técnica Superior de Ingeniería
Universidad de Sevilla

Sevilla, 2016

Trabajo Fin de Grado
Ingeniería Aeroespacial

Numerical Analysis on DEFORM-3D of limit strains in Single Point Incremental Forming for AISI304-H111 sheets

Autor:
Álvaro Fernández Díaz

Tutor:
Gabriel Centeno Báez
Profesor Contratado Doctor

Departamento de Ingeniería Mecánica y Fabricación
Escuela Técnica Superior de Ingeniería
Universidad de Sevilla
Sevilla, 2016

Proyecto Fin de Grado: Numerical Analysis on DEFORM-3D of limit strains in Single Point Incremental Forming for AISI304-H111 sheets

Autor: Álvaro Fernández Díaz

Tutor: Gabriel Centeno Báez

El tribunal nombrado para juzgar el Proyecto arriba indicado, compuesto por los siguientes miembros:

Presidente:

Vocales:

Secretario:

Acuerdan otorgarle la calificación de:

Sevilla, 2016

El Secretario del Tribunal

A mis abuelos

Agradecimientos

A mis padres, porque sin su apoyo no habría podido llegar a estudiar esta carrera.

A mis amigos, por aguantarme y apoyarme en cada paso del camino.

A mi tutor Gabriel Centeno Báez, por haberme permitido realizar este proyecto con él, a pesar haber estado fuera, y de lo apretado de su agenda, y por su disposición a sacar un rato para ayudarme y resolverme las dudas siempre que le era posible.

A los miembros del departamento de Ingeniería Mecánica y Fabricación, especialmente a Marcos Borrego Puche, fundamental apoyo en mis primeros pasos con DEFORM™-3D, y a Andrés Jesús Martínez Donaire, por estar siempre dispuesto a ayudarme con cualquier duda que me surgiese.

A mi profesor del Bachillerato Internacional Jesús Moreno, por mostrarme el maravilloso mundo de la física y la ingeniería.

Y finalmente, a mi compañero y amigo Pedro Grau Morgado, por su apoyo y camaradería estos años, y por demostrarme que con empeño y dedicación, todo es posible.

Álvaro Fernández Díaz

Sevilla, 2016

Resumen

El principal objetivo de este proyecto es crear un modelo numérico para placas de acero AISI304-H111 conformadas mediante procesos de conformado incremental mono-punto (SPIF), y validarlo en términos de deformaciones con los resultados experimentales obtenidos previamente por el grupo de investigación del Área de Ingeniería de los Procesos de Fabricación del Departamento de Ingeniería Mecánica y Fabricación de la Universidad de Sevilla. El modelo se realizará en DEFORM™-3D, conocido por ser un software robusto basado en la mecánica de los elementos finitos (FEM), que usa cálculo implícito y tiene una gran aplicación industrial.

El documento está estructurado en tres secciones principales. Comienza comentando los distintos métodos de conformado incremental de chapas (ISF), describiendo con más detalle las características y aplicaciones del SPIF, para acabar estableciendo los principales objetivos del proyecto y revisando los antecedentes experimentales.

La segunda sección es un conciso manual paso a paso que enseña cómo usar DEFORM™-3D, concretamente cómo crear el modelo numérico para los procesos de conformado incremental llevados a cabo en este proyecto.

Finalmente, en la tercera sección, se exponen los resultados y se analizan en términos de deformaciones, para compararlos con los resultados experimentales previamente mencionados, validando así el modelo.

Abstract

The main objective in this project is to create a Single Point Incremental Forming (SPIF) process numerical model for AISI304-H111 sheets, and validate it in strain terms with experimental data previously obtained by the group of Manufacturing at the Department of Mechanical Engineering and Manufacturing at the University of Seville. The model will be carried out on DEFORM™-3D, which is known for being a robust FEM-based software, having a great industrial application and using implicit computation.

The document is structured in three main sections. It starts by commenting different ISF methods, describing in more detail the characteristics and applications on the SPIF, to finish by establishing the main objectives of the project, and reviewing the backgrounds.

The second section is a concise step by step manual guide to show how to use DEFORM™-3D, specifically how to create a numerical model for the incremental forming processes carried out in this project.

Finally, in the third section, the results were exposed and analysed in strain terms, in order to compare them with the previously commented experimental results, validating the model.

Index

1 Tables Index

2 Figures Index

1 INTRODUCTION

Sheet forming in current industry is a high used process among a large group of production sectors, so that it's in continuous progress and revision.

For example, in the aeronautical sector, sheet stretching is used to form the body of the aeroplanes, needing high specialized equipment and tools. That's why this technology is only profitable with a large scale of production.

Incremental sheet forming is an innovative process that fulfils the current requirements for flexible, sustainable and economic manufacturing technologies viable for small and medium-sized batches, not being necessary the use of expensive dedicated machines or equipment.

Single-Point Incremental Forming (SPIF) is the simplest manufacturing process among those based on incremental forming of a metal sheet. It consists on a hemispherical end forming tool driven by a Computer Numerical Control (CNC) machine that follows progressively a pre-established trajectory, deforming plastically a peripherally clamped sheet blank into a final component, without the use of a forming die during the process. That allows a better formability, plus the other advantages formerly mentioned.

This Project will calculate numerically with a Finite Element Method (FEM) program, DEFORM™-3D, the strain evolution on an AISI304 sheet, with 10mm and 20mm tools. That, under some hypothesis, will allow to have a model to compare with experimental results obtained by Centeno et al (2014), and also provide the stress distribution on the sheet.

1.1 Forming Limit Diagram

The main used tool to measure the formability of a metal sheet is the Forming Limit Diagram, proposed by Keeler and Backhofen (1963), and Goodwin (1968). This diagram depicts the Forming Limit Curve, which shows mayor and minor principal strains limit values in the sheet plane, needed to create the failure under different strain relations.

Marciniak (2002) established that the formability is related with the strain state. If it's assumed that the total sum of the three mayor strains, $\varepsilon_1, \varepsilon_2, \varepsilon_3$ equals zero, because of volume constancy, plus it's only needed to know two of them, related by the following expression:

$$\varepsilon_2 = \beta \varepsilon_1$$

There are several strain cases of interest, distinguished by the value of β, as explained:

- $\beta = 1$, in this case, $\varepsilon_1 = \varepsilon_2$, with constant strain in every direction in an equi-biaxial state.
- $\beta = 0$, there is no minor strain, $\varepsilon_2 = 0$, being known as plane-strain.
- $\beta = -0.5$, this is the state present in tensile tests of isotropic materials, known as uniaxial.
- $\beta = -1$, here $\varepsilon_1 + \varepsilon_2 = 0$, and consequently, $\varepsilon_1 = 0$, there is no variation in the thickness. This state is known as deep drawing.

These states are represented in the following figure:

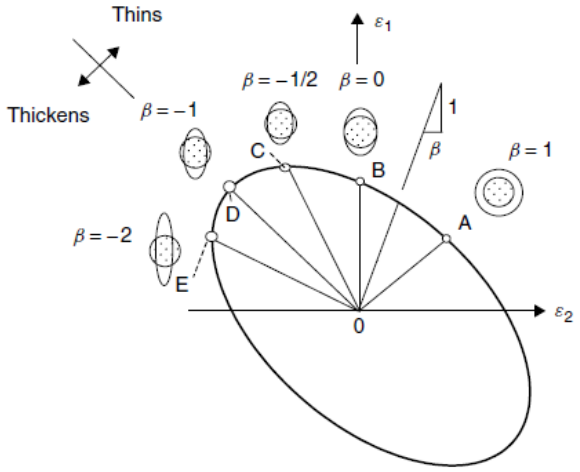

Figure 1.1 *Different states of the principal strains*

The FLC usually shows a necking failure curve, generally in ductile materials. In *Figure 1.2* can be seen the evolution of that curve for different materials. It's worth to mention that the lowest value of the curve, known as FLC(0), is a characteristic data of the material, which occurs under plane strain conditions.

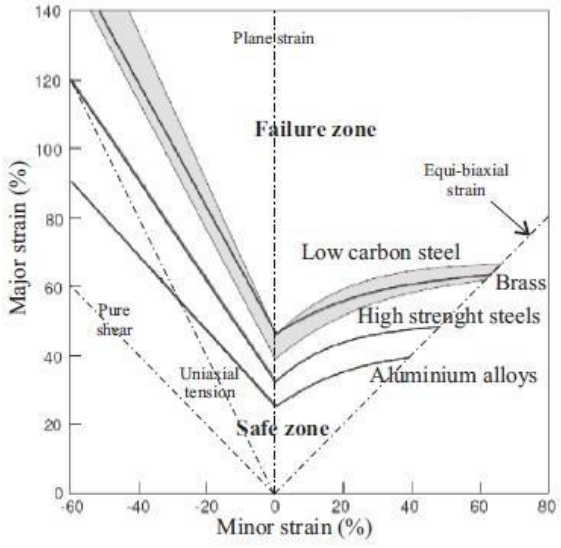

Figure 1.2 *Different states of the principal strains*

Plus it's usually added a ductile fracture curve above the necking curve. As it depends on the ductility of the material, on very ductile materials it will be a decreasing straight line, while in low ductility materials will be similar to the necking failure curve, approaching to equi-biaxials strain conditions, and therefore showing that the material will reach fracture with almost no necking.

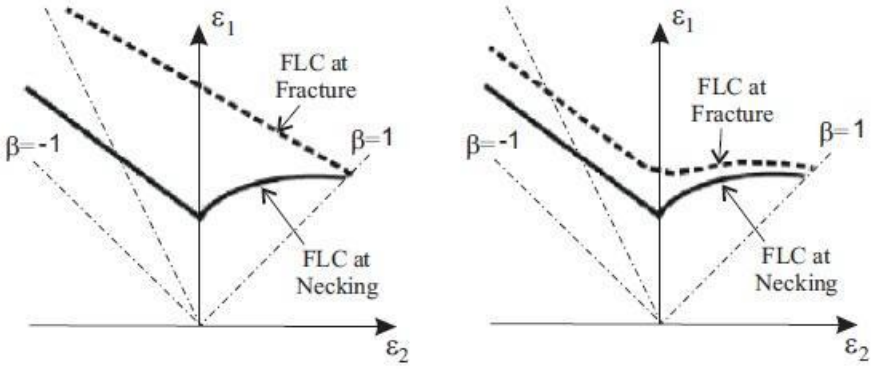

(a) (b)

Figure 1.3 *FLC curves for high ductility* (a) *and low ductility* (b) *materials*

Nowadays, the numeric computer calculation for both the numeric evaluation of the sheet forming process and the numeric estimation of the FLD, allowing then to compare it with the experimental curves. For good results on the forming diagrams, several experimental tests, and simulations to contrast results. These tasks are necessary to create a failure criterion of the material that allows forming in a safe strain range. That's why this project will simulate something already analysed experimentally.

There is a wide variety of ductile fracture criteria on scientific literature. Some studies proved that continuous fracture criteria (integral criteria) predict correctly the lineal FFL. However, those criteria are not capable of reproduce the seen FFL for low ductility metal sheets, with either a V-shaped curve or a complex form in the necking area. In those cases, it has been proved that failure criteria based on tangential stresses, such as Tresca or Bressan approximates well the experimental FFL in a wide range of strain relations. Those diagrams will be obtained performing several tests, such a stress tests, stretching tests and stretch-bending tests. One example of an experimental Forming Limit Diagram is the one obtained by the previously mentioned paper (on which this project is based), Centeno et al. (2014):

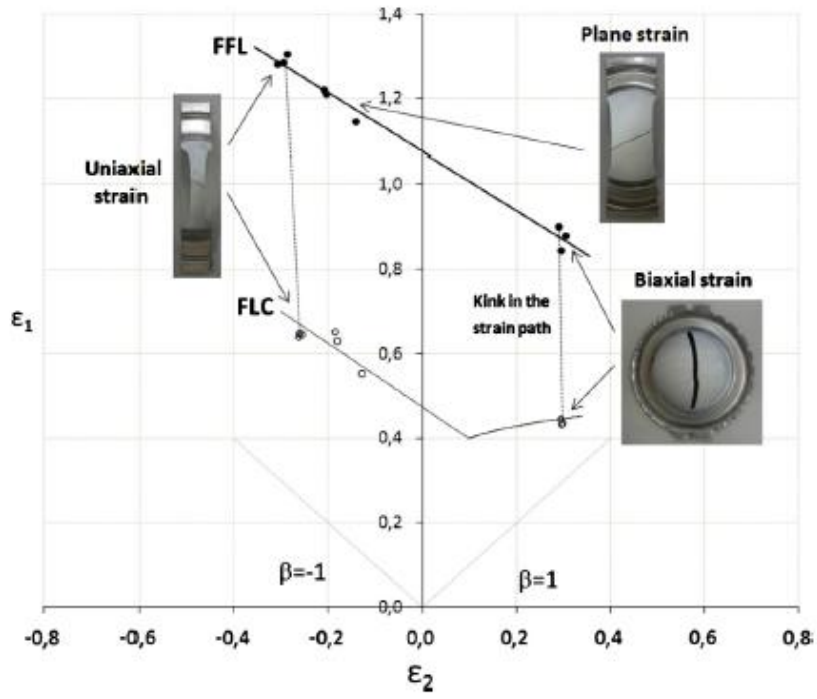

Figure 1.4 *Forming limit diagram (FLD) based on conventional Nakazima tests containing the forming limit curve (FLC) and the fracture forming line (FFL) for 0.8 mm thickness AISI 304 metal sheets*

1.1.1 The Nakazima stretching test

This test consists on taking a previously prepared sample and setting it in the blank holder. Then, the top die is placed on the sheet sample and secured to hold the system. Then a previously lubricated hemispherical punch of 100 mm of diameter rises at constant speed to form the sample until failure occurs.

This is the most used stretching test, being used as a reference on the ISO12004-2, which standardizes the construction of forming limit curves (FLC) on laboratories, both on the testing parameters and the methodology to detect the onset of localised necking. This part of the ISO12004 specifies the testing conditions to be used when constructing a forming limit curve (FLC) at ambient temperature and using linear strain paths.

The considered material is flat, metallic and of thickness between 0.3 mm and 4 mm, being the recommended thickness for steel of 2.5 mm. It also standardizes the rest of the test conditions, such as lubrication, punch velocity or specimen geometries. Regarding the geometry, it's recommended to use notched specimens with a calibrated central part, with a 25% bigger length than the punch diameter.

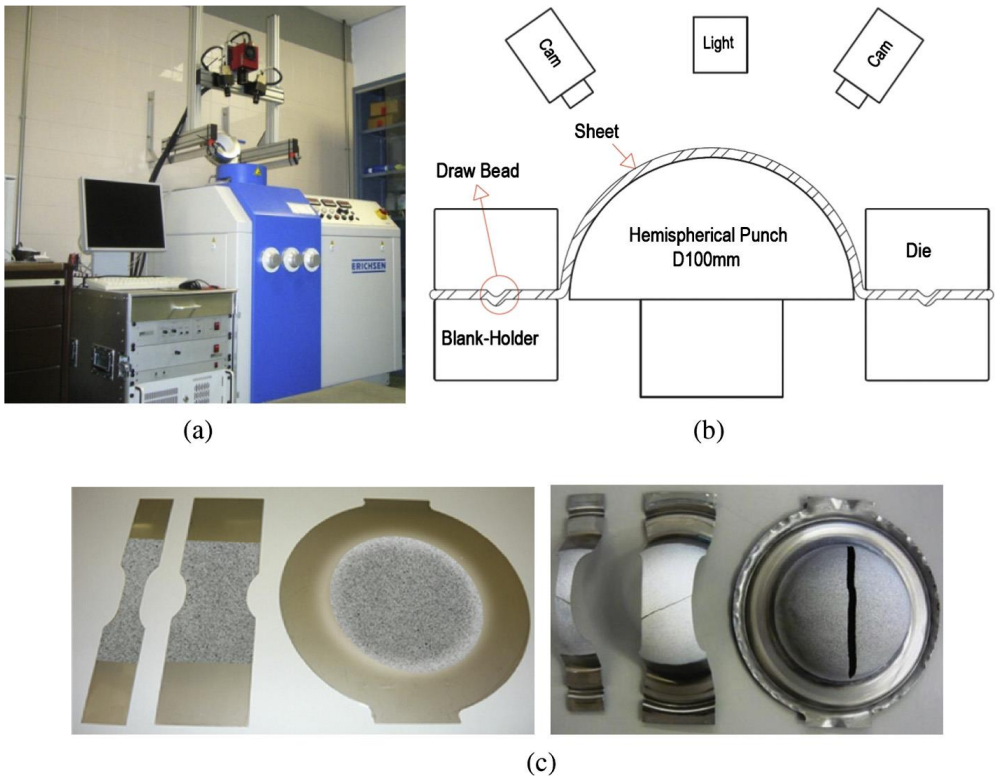

Figure 1.5 (a) *Erichsen universal sheet metal testing machine,* (b) *scheme of the experimental setup and* (c) *specimen geometries before and after testing*

1.2 Incremental sheet forming processes

Just as Schmoeckel (1992) predicted, automatization has made forming processes more flexible.

The ISF deforms gradually a metal sheet with one only tool, guided by a Computer Numeric Control machine, allowing to obtain many different geometries. It allows fast prototyping, needing short times on design and manufacturing. That makes those processes very profitable for the production of small batches of pieces.

Nowadays there are plenty of different metal forming processes that use an incremental approach. As said before, in those processes the material forming is produced incrementally, and only in a small area of the sheet, therefore needing smaller forces compared to traditional processes. Now some of them will be commented.

1.2.1 Spinning

In the spinning, the metal sheet is embedded on a spinning mandrel. While the sheet is rotating, the tool approaches progressively forming it to the desired geometry. The tool has a roller geometry, and can be actuated either manually or mechanically (a lathe is needed for that). This is one of the oldest processes, being created in the Middle Age.

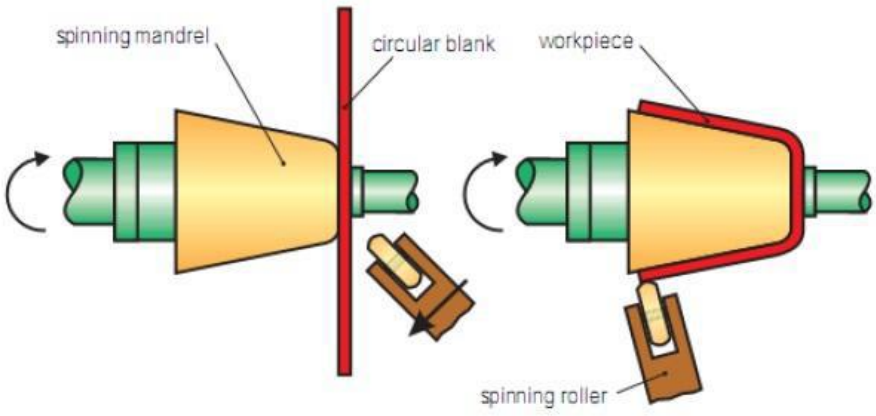

Figure 1.6 *Spinning schematics*

There is a variant, known as *shear spinning*, where the sheet isn't bent, but stretched, reducing its thickness, fulfilling the Sine Law:

$$t_f = t_0 * sen\left(\frac{\pi}{2} - \alpha\right)$$

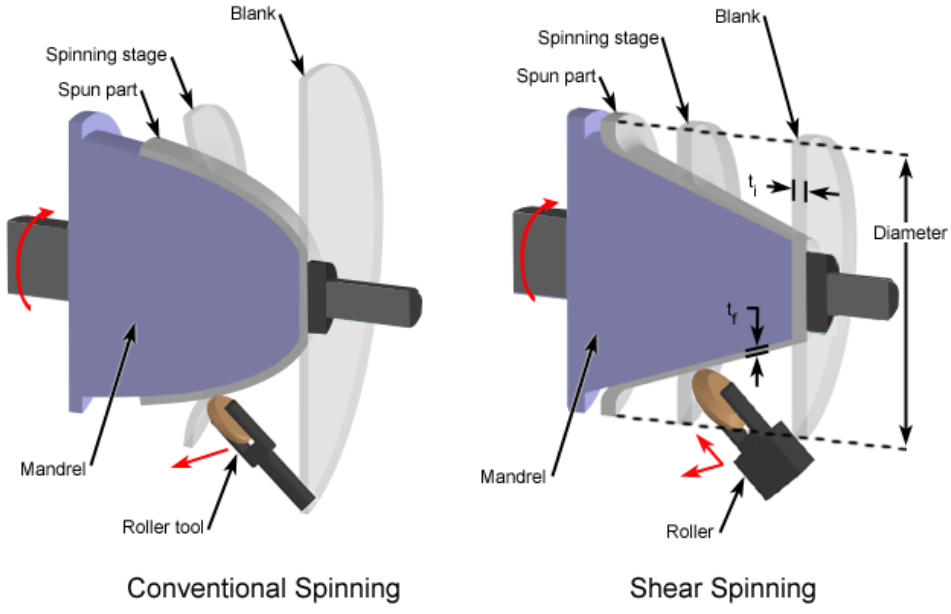

Figure 1.7 *Structural differences between conventional and shear spinning*

1.2.2 Single Point Incremental Forming (SPIF)

The idea of gradually forming with only one point tool was already patented by Leszak (1967), which was a visionary, since in that time it wasn't possible to do it. Single Point Incremental Forming process is a great progress compared to spinning, because it allows to create not axisymmetric geometries. In this process, the metal sheet is held between a blank holder and a backing plate. The tool will be controlled by a CNC machine, and it moves along the designed trajectory to describe the final geometry of the desired piece. In this process,

there is no die supporting the outer side of the sheet.

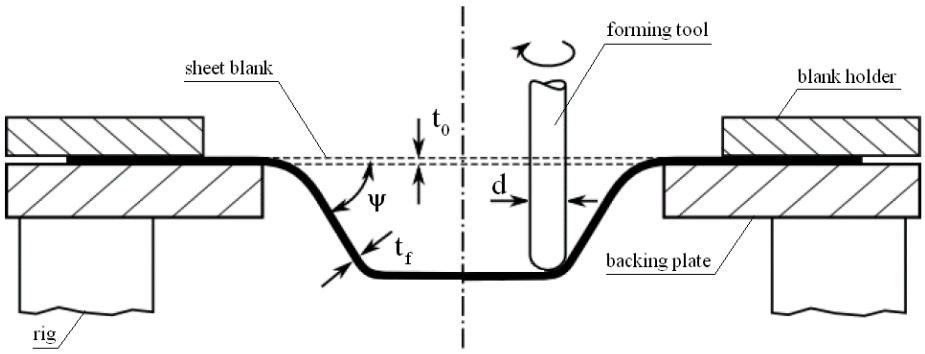

Figure 1.8 *Schematic representation of a SPIF process*

1.2.3 Incremental Forming With Counter Tool (IFWCT)

The Incremental Forming with Counter Tool, as its name says, differs from the SPIF in the presence of an auxiliary tool that is located in the same point of the main tool, but on the other side of the sheet, and follows the same trajectory.

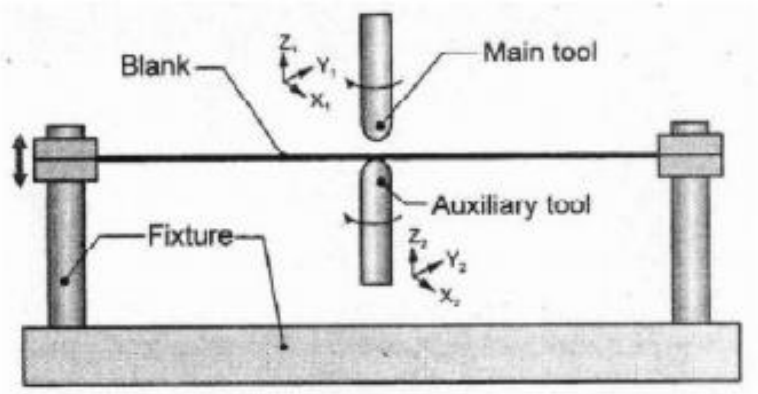

Figure 1.9 *Schematic representation of an IFWCT process*

1.2.4 Two Point Incremental Forming (TPIF)

The TPIF process is very similar to SPIF, being formed on the outer side of a metal sheet by a single tool, but it is distinguished from the SPIF by its use of a partial or total die, or a second tool, that unlike the IFWCT process, doesn't follow the trajectory of the main tool, but it is just adjusted in the vertical direction when needed.

It has two typical categories:

- With partial die, that serves as the backing plate from the SPIF process, but providing a better geometric accuracy
- With total die, that serves as mandrel or positive matrix, allowing an even better finish.

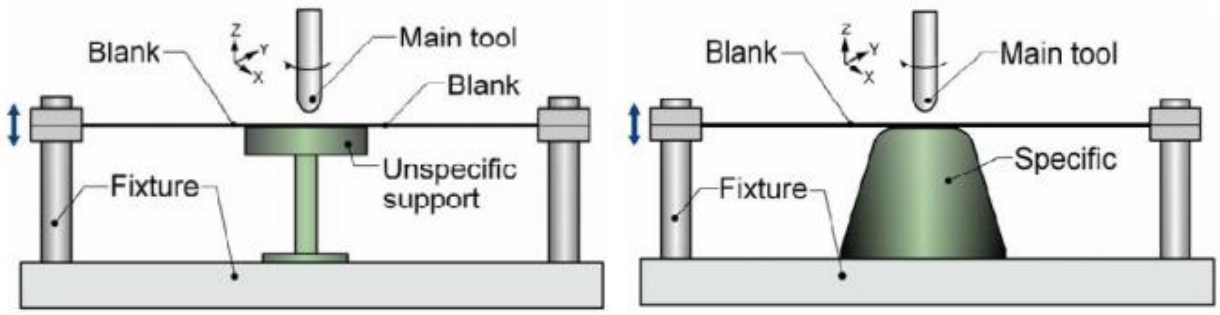

(a) (b)

Figure 1.10 *TPIF schematics with* (a) *partial die and* (b) *total die*

1.2.5 Multistage Forming

For each specific material and thickness sheet, the maximum forming angle can be easily obtained in a test where the final geometry is a cone with variable generatix angle, keeping constant the rest of the variables. It's easy to check that it's impossible to produce pieces with right angles, because according to the Sine Law, its final thickness would be zero.

One way to enhance this angle is to increase the initial thickness of the sheet, but it would create problems, in the formability and in the necessary loading capacity of machines and tools. The step down and the tool diameter also affects, but the mainly final solution was to generate trajectories with several stages in which the forming angle is being increased.

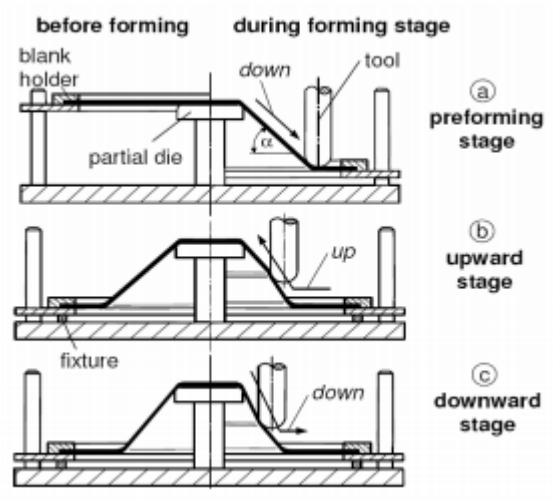

Figure 1.11 *Multistage forming example*

Recently, Skjoedt et al. (2008) proposed a solution to obtain vertical walls cones based on this process, realized with 5 stages:

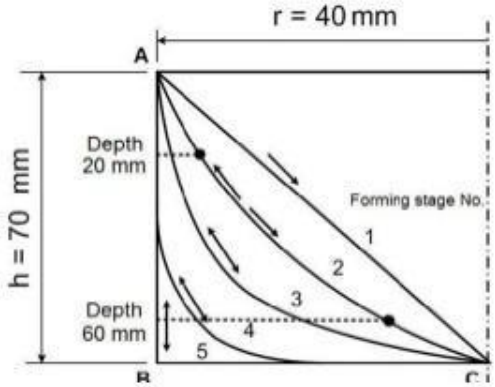

Figure 1.12 *Multistage strategy formulated by Skjoedt et al. (2008)*

Also, Duflou et al.(2005) used multistage forming strategies in order to create geometries without revolution axis.

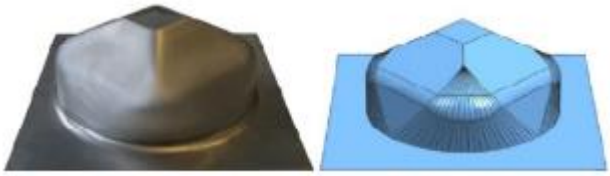

Figure 1.13 *Geometry without revolution axis achieved with multistage forming.*

1.3 Single Point Incremental Forming characteristics

1.3.1 The forming tool

The main element in this process is the solid tool with a semi spherical tip, which assures a continuous contact in the sheet point where it's plastically formed. In some cases, with sharp wall angles, might be needed a smaller stem than the tool diameter of the spherical tip, avoiding that way the contact between the stem and the sheet.

In most cases, these tools are made of steel. Since the biggest heat source is friction, to reduce it, and therefore increase its useful life, it's usually lubricated. It can be covered or even totally made by some material with greater hardness, such as cemented carbide, reducing the tool weathering.

A wide range of tool diameters is used, going from small diameters of 6 mm to 100 mm of diameter, used this last one to manufacture larger pieces. Naturally, they need much more power due to the much bigger contact angle. It affects the final surface finish and the manufacturing time, being the tool diameter determined by the smallest concave radius required in the geometry.

Figure 1.14 *SPIF forming tool*

1.3.2 The blank holder

The blank holder is used to firmly hold the sheet during the forming, restricting the displacement. It also has a backing plate, which guides the sheet material in the correct direction in the process. As mentioned before, in the TPIF case, the die (that works as backing plate), can move along the vertical direction.

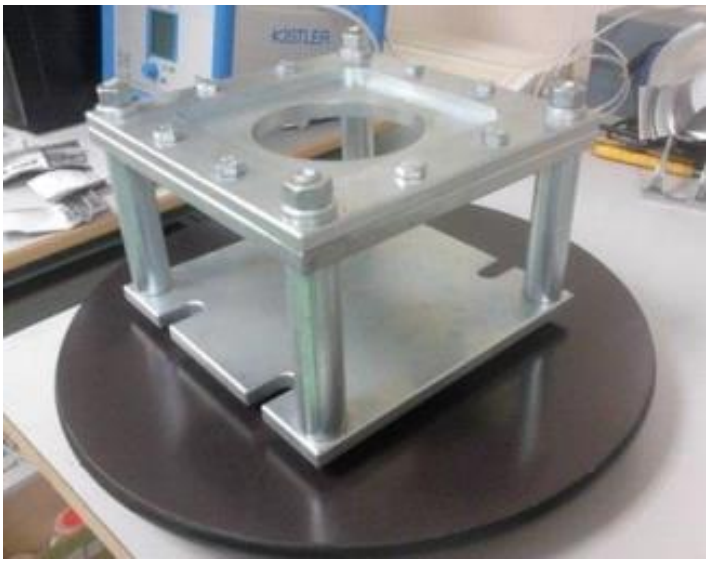

Figure 1.15 *Blank holder and backing plate used in a SPIF process*

1.3.3 Incremental Forming machinery

In SPIF processes, the main force applied is the axial one, needing a previous estimation to ensure the correct behaviour of the machine. Usually, any 3-axial CNC machine is suitable to form in SPIF.

Figure 1.16 *3-axial CNC machine*

Their high velocities, allowing large workloads and stiffness make them ideal for SPIF. There are different designs, differing on their workload, maximum velocity, maximum load, stiffness and cost, allowing to choose the necessary one according to the necessities.

Nowadays, there is only one company that has created a specifically designed SPIF machine (Hirt, 2004). It has a high feed rate and allows medium sized workloads. It's based on the technology developed by Amino et al. (2002) including an Aoyama et al. (2000) patent:

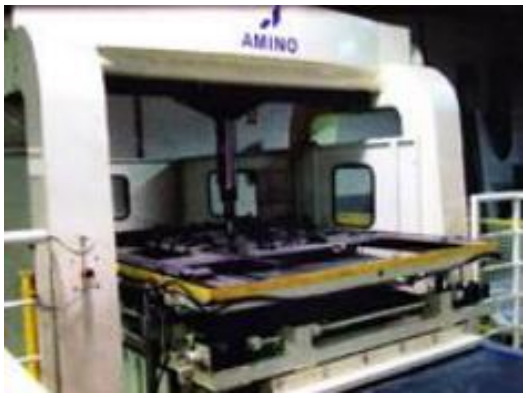

Figure 1.17 *SPIF dedicated machine*

There are plenty other machines potentially suitable. Industrial robots are being tested (*Figure 1.18*) that admit huge workloads, low stiffness and acceptable maximum loads. Several institutes are trying to apply industrial robots to incremental forming such as Schafer et al. (2004) and Meier et al. (2005). This forming method is yet in its primary phase. One special setup in robot forming is to use incremental hammer fisting instead of a continuously moving rigid tool. In this case, the forming tool describes a fast oscillating movement, which gives the desired geometry to the sheet.

Figure 1.18 *Robotic Incremental Sheet Metal Forming*

The Stewart platform (Stewart, 2005) allows infinite degrees of freedom. It's not being used, but it has a wide potential compared with 5-axis milling machines.

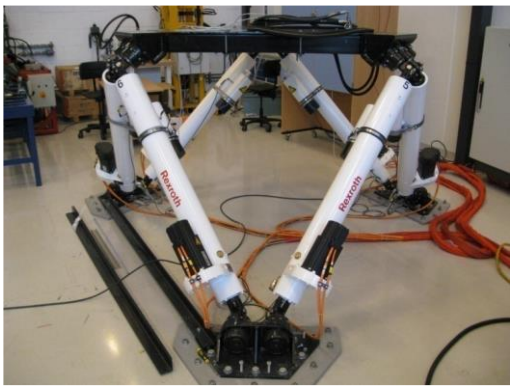

Figure 1.19 *Stewart Platform*

1.3.4 SPIF's advantages and disadvantages

SPIF's main advantages are:

- Parts production directly from a CAD archive.
- No need for positive or negative matrix.
- Parts dimensions are only limited by the machine.
- Design changes can be performed quickly and easily.
- Increase of materials formability.
- Can be realized in a conventional CNC machine.
- Due to the incremental nature of the process, the required loads are small.
- A good surface finish can be achieved.

Regarding its disadvantages, the following can be mentioned:

- Longer processing time compared with conventional deep drawing.
- Limited to small production batches.
- The creation of right angles must be achieved by several stages.
- Worse geometric accuracy, especially in edges and convex bending radius.
- There is elastic recuperation, although it can be minimized using some specific correction algorithms.

1.4 Background

The increase of the formability of metal sheets with ISF processes, specifically Single Point Incremental Processes, has been experimentally studied by several authors, such as Emmens et al. (2009), Jeswiet et al. (2010) or Silva et al (2011) among others.

The Fabrication Engineering Process investigation group from the Seville's University Mechanic Engineering Department has been researching and performing numerous tests and numeric simulations about metallic sheet forming, specifically the influence of the flexion in forming processes, evaluating failure mechanisms and researching what parameters affect them, as in Centeno et al. (2012).

Under that line of research, a methodology has been developed to obtain limit forming diagrams, for both stretching, and stretching with flexion situations. That methodology has been tested for several materials, such as AA7075-O, AA2024-T3, or AISI304-H111 among others.

Specifically, that last material will be analysed in this project. In Centeno et al (2014), there was obtained the following strain evolution on SPIF on the outer surface of the AISI304 sheet, once the failure took place.

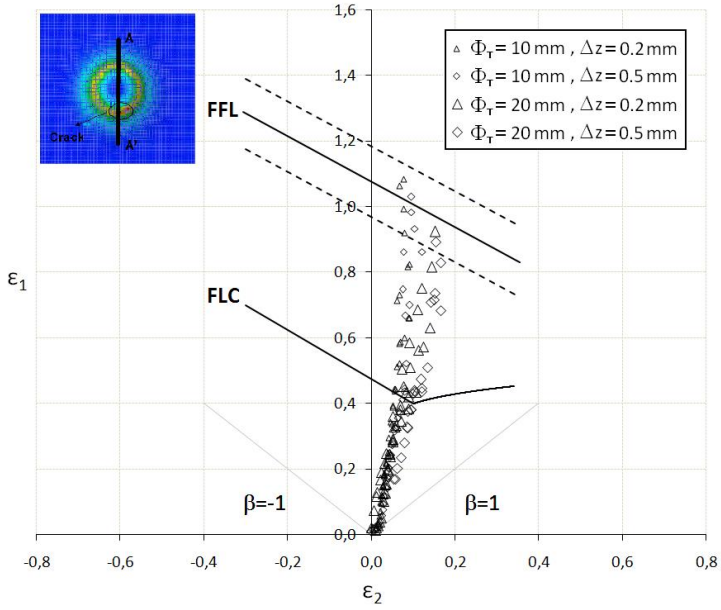

Figure 1.20 *Spifability of the AISI 304 metal sheets using tool diameters of 10 and 20 mm for step downs of 0.2 and 0.5 mm per pass.*

Several different tests were carried out, with tools of 6mm, 10 mm and 20 mm diameter. For each tool diameter, the step down was alternatively set to 0.2 mm and 0.5 mm per pass. Three replicates of each SPIF test were carried out, that gave almost the same results.

The final strain state was measured with ARGUS®, and the fracture strains were obtained measuring the sheet thickness along the crack at both sides of the final cut.

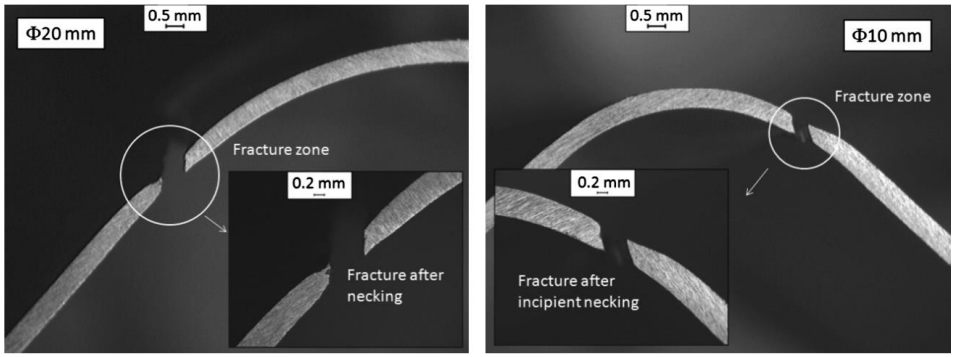

Figure 1.21 *Fractography of the failure zone in stretch-bending using a cylindrical punch of 20 mm (left) and 10 mm (right) diameter, respectively.*

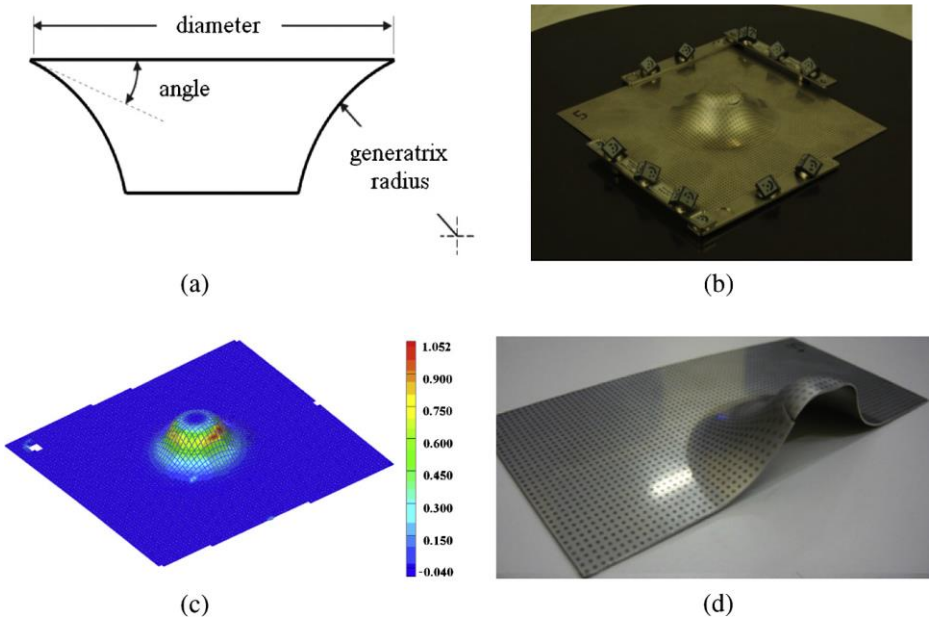

Figure 1.22 (a) *Testing geometry used in SPIF,* (b) *point pattern on the final part and* (c) *contour of major principal strain obtained from ARGUS® and* (d) *cut final part ready for measuring thickness along the crack.*

As shown in *Figure 1.20*, it can be seen a great enhancement in the formability of the AISI304 sheets, allowing stable plastic deformation until values of major principal strain well above de FLC, and near the FFL. Specially, in the case of a 10 mm diameter tool, the principal strains reach the FFL within stable deformation. In that case, the major principal strain reach values up to 1.1 of logarithmic strain placed nearly above the FFL determined in Nakazima tests.

1.5 Project's objectives

The main objective in this project is to accomplish a numeric analysis based on a Finite Element Method model in DEFORM™ -3D. The model will consist on a 0.8mm AISI304-H111 sheet, being formed with different diameter tools, following the real path used in the experimental processes done by Centeno et al. (2014) previously commented.

The tools will have a diameter of 20 mm and 10 mm respectively, and the step down in all the simulations will be set to 0.5 mm, to reduce 2.5 times the computing time over the 0.2 mm step down case, and still being able to compare the simulation with the experimentation.

Once accomplished the numeric model, and being proven its proper functioning until the failure depth in both tool diameter cases, several particular objectives were set:

- Creation of a *step by step* manual to model the incremental forming processes using DEFORM™-3D.
- Evaluation and validation of an efficient numeric model that provides good results without long computing times.
- Analysis of the numeric model's limits.
- Analysis of the principal strains in the sheet until the failure within the results of the AISI304 Forming Limit Diagram, assuming the final depth for the simulation, the average depth where the failure took place in the experimental SPIF processes.
- Failure prediction based in the Ayada accumulated damage criterion.

2 DEFORM™-3D

This chapter describes the necessary steps in order to create the DEFORM™-3D models for the requested analysis.

DEFORM™-3D is a simulation processor system, designed to analyse a 3-dimensional flux in metal forming. It provides the material flux, without the delays and costs related to the real analysis. It has proven to be a strong solution on the industrial environment for two decades.

DEFORM™-3D allows to import geometries from CATIA, and its integrated FEM program allows to predict the fracture in multiple processes, such as rolling, extrusion, die forming, indenting, etc.

The Automatic Mesh Generator creates and optimizes the mesh system where the local element size is specific for the analysed process. It also has a *user defined* system that allows the user to specify the mesh density wherever is needed, and an automatic remeshing system, capable of creating a variable-sized mesh, making into smaller in complex locations, and automatically remeshing when needed (or following some pre-specified parameters).

That is one of the main advantages of DEFORM™-3D compared to other FEM programs. That's why despite being based on implicit calculation, it has much shorter computing time and numeric requirements. Besides, it gives the opportunity of importing and exporting data in the *post-processor*, such as results, geometries, routines, etc.

2.1 DEFORM™-3D as a numeric tool.

First of all, a folder where the simulation will be stored must be created, making sure there is enough free space to store the results. As the program is working, it will be generating 2GB databases until it goes through all the steps programmed.

In order to create the simulation, it's needed go to the *pre-processor*.

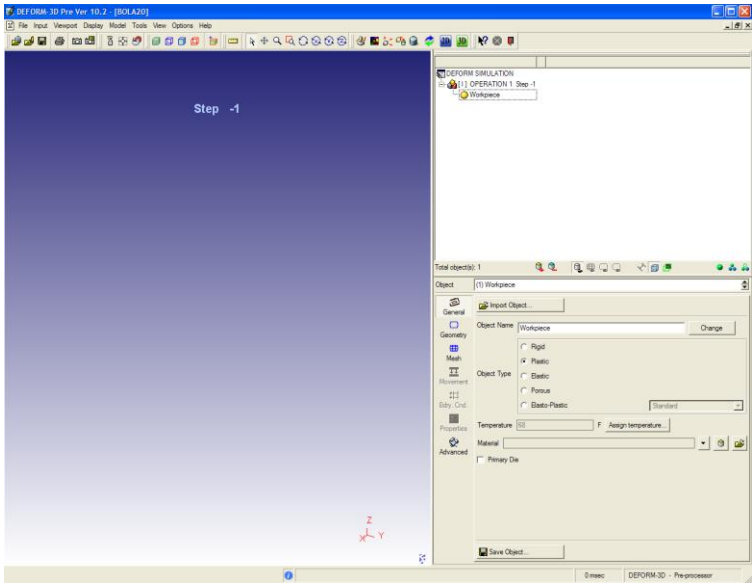

Figure 2.1 *Pre-processor*

The top right tree shows the number of pieces in the simulation, and (later on, when the mesh will be created) it shows its material and mesh.

Once in the *pre-processor*, the program has to be adjusted to operate in SI variables. For that, Simulation Controls must be selected in the top toolbar, and then the SI option.

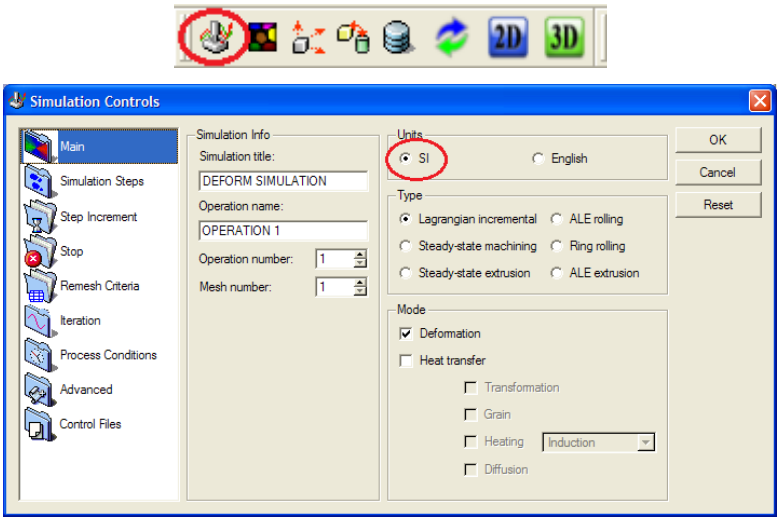

Figure 2.2 *Simulation Controls (SI units)*

After that, the material of the metal sheet will be created. In our case, it's a sheet of steel AISI304-H111. To create it, in the *material* icon has to be clicked, in the main toolbar:

Figure 2.3 *Main toolbar on the pre-processor*

DEFORM™-3D has a predefined material database, where the AISI304 is included, so it has to be imported, and modified in order to be adjusted with the experimental mechanical properties shown in *Table 2-1*.

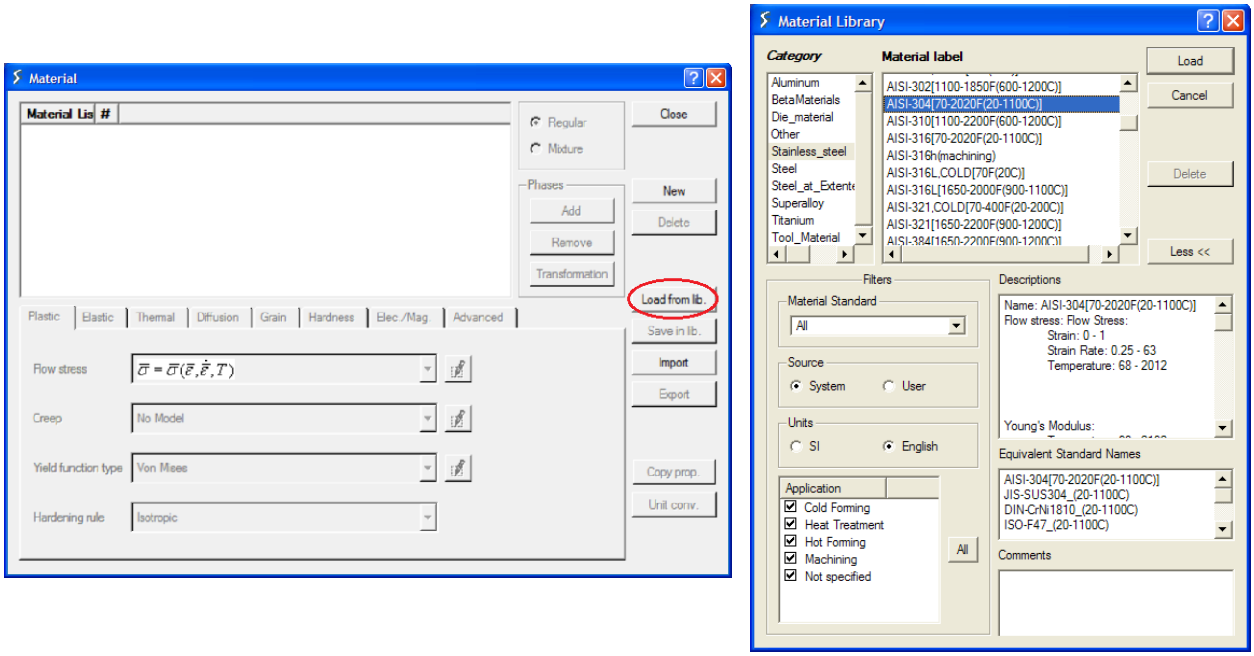

Figure 2.4 *Material window*

However, as shown in Centeno et al. (2014), it is needed a different mechanical characterization from the predefined in the program. Specifically, in this characterization, the plastic behaviour of metal sheets fits a Swift's law as follows, with the mechanical properties summarized in *Table 2-1*.

$$\bar{\sigma} = K(\varepsilon_0 + \bar{\varepsilon}^P)^n$$

Table 2-1 *Mechanical properties of the AISI 304 metal sheets*

UTS(MPa)	$\sigma_{y0.2}$(MPa)	E(GPa)	K(GPa)	N	ε_0
669	503	207	1.55	0.594	0.055

For that, a Norton-Hoff Law will be adapted as follows:

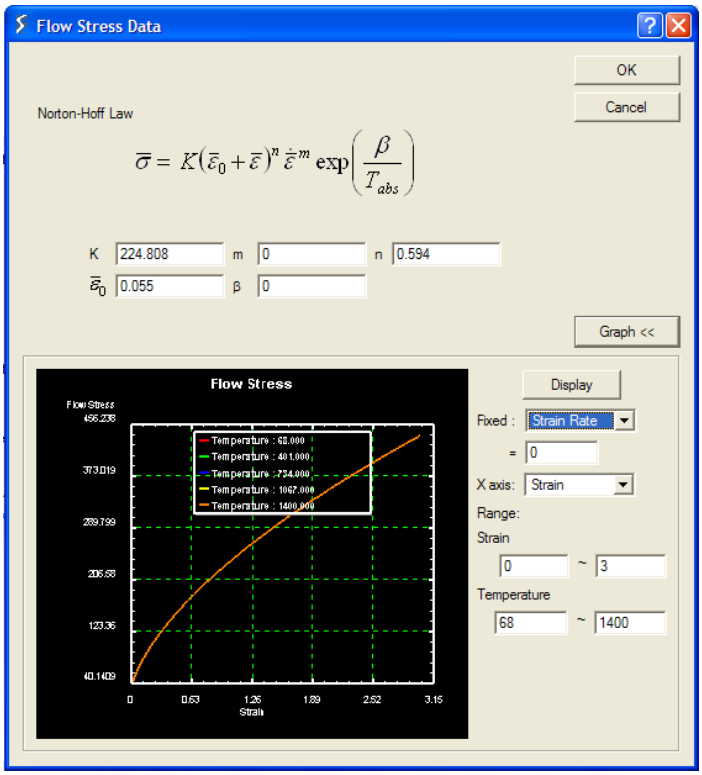

Figure 2.5 *Behaviour law generator*

Finally, the fracture method to Ayala must be set in the main material window, adjusting the mechanic limit to 0.9.

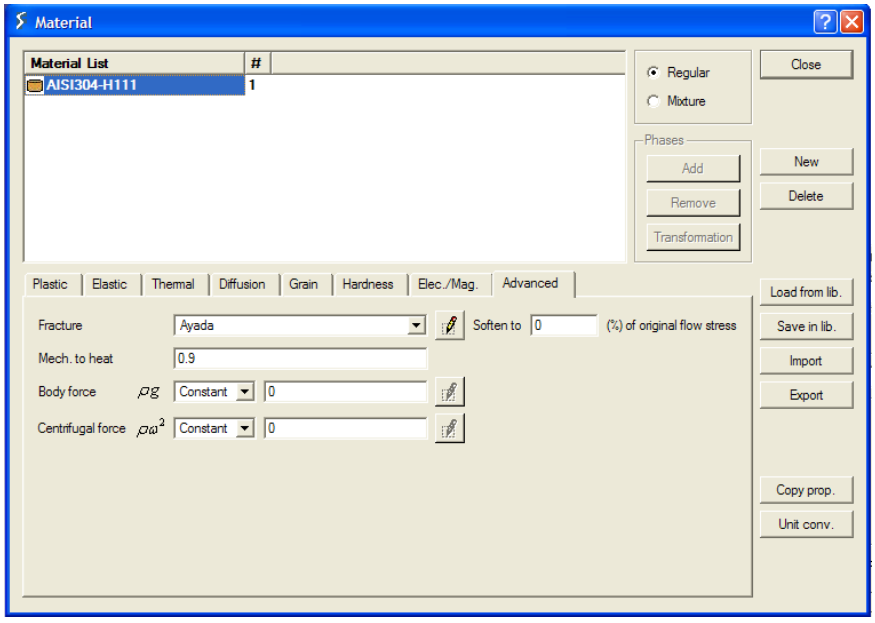

Figure 2.6 *Fracture method*

Once the material is created, next step is to create the different pieces of the simulation. For the metal sheet, the elasto-plastic option will be chosen, and in the material option, the AISI304 previously created will be set:

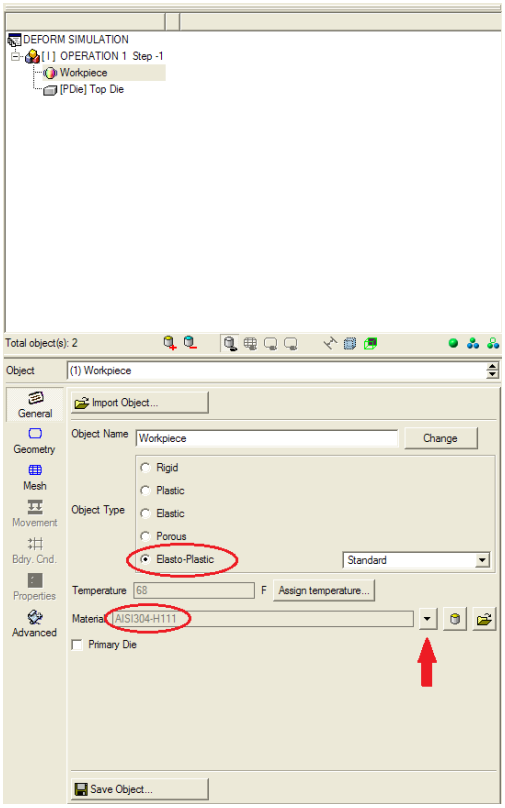

Figure 2.7 *Object type and material choosing*

Then the geometries for the sheet and the tool will be created. Note that there is no blank holder. That's because with blank holder, the program has problems with the boundary conditions (as it will be discussed later).

To create the geometries, the *Geo Primitive* option will be selected, and the values will be introduced in mm in the subsequent window.

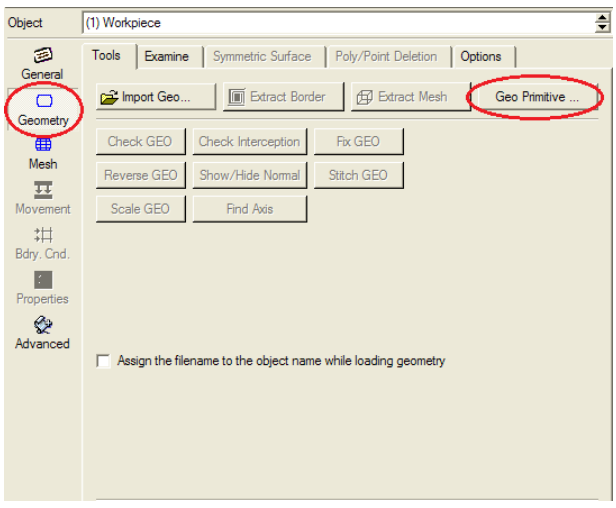

Figure 2.8 *Geometry selection*

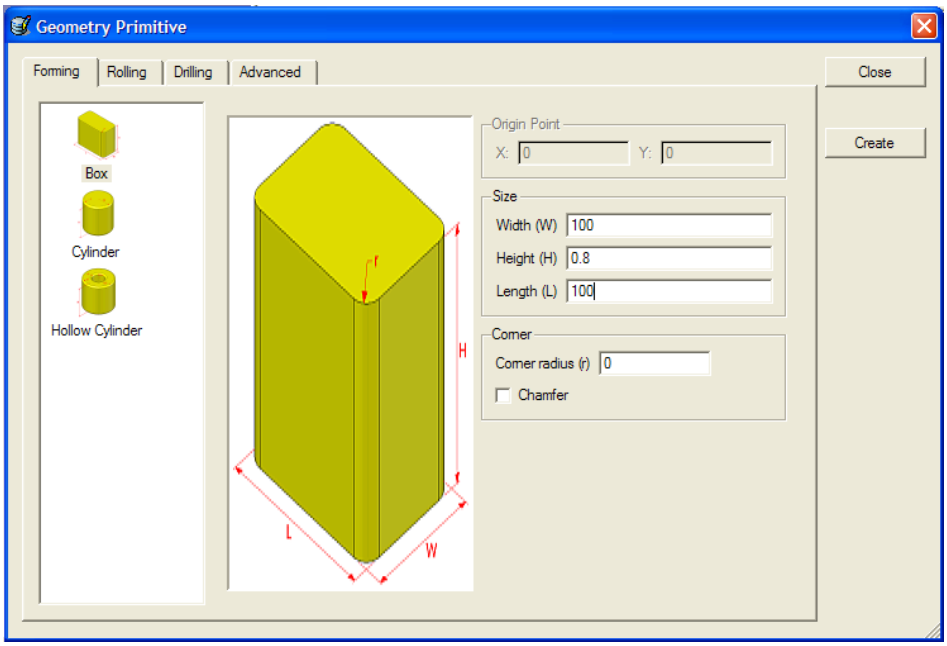

Figure 2.9 *Sheet geometry data*

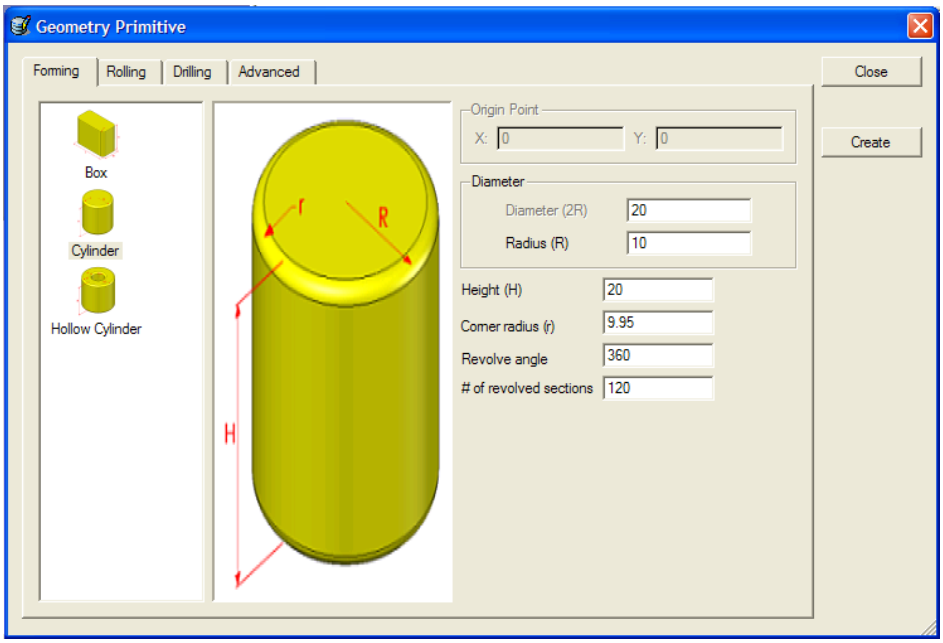

Figure 2.10 *Tool geometry data*

Then it is needed to adjust the position of the different pieces to locate them properly and generate the interactions between them with the object positioning option in the main toolbar.

Figure 2.11 *Main toolbar on the pre-processor*

As both pieces overlap each other, they need to be separated a bit, and after that make them interfere. For that first will be used the *drag* option, that allows moving the object in any direction. In this case the tool will be moved in the Z direction:

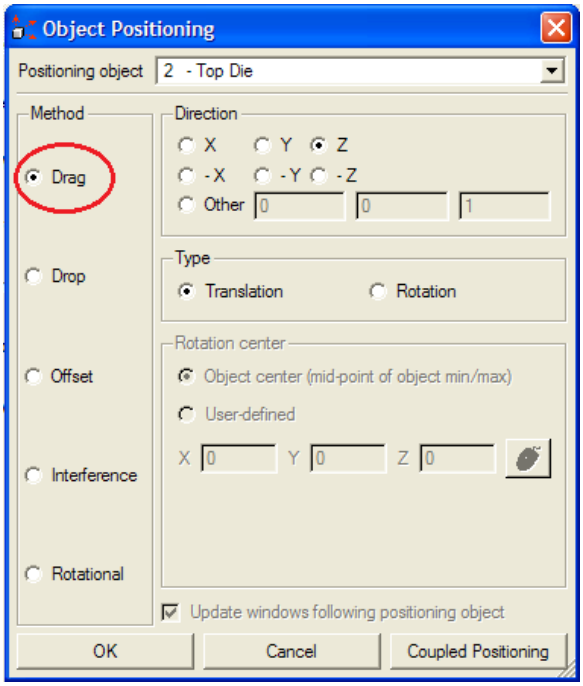

Figure 2.12 *Pre-processor drag control*

After that, the option *interference* is used to bring them closer and make them coincide in one point. Notice that the *drop* option could be used too, but for this project was used *interference* so that the rotation of the tool doesn't affect (although it wouldn't affect anyways, because it's a solid of revolution).

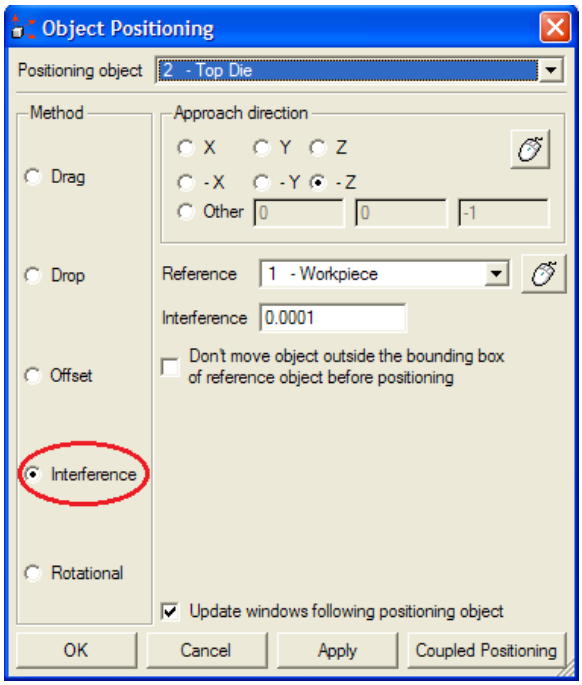

Figure 2.13 *Pre-processor interference control*

With all set, the final geometry is as follows:

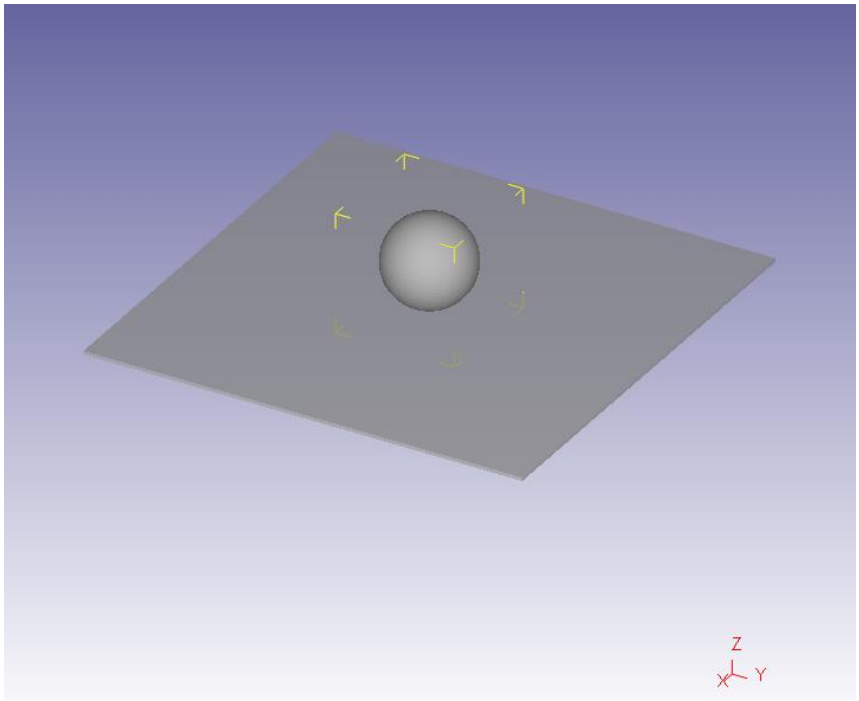

Figure 2.14 *Simulation geometry correctly positioned*

With the geometry set, the meshing will be created. The Automatic Mesh Generator distributes the mesh to adjust it to the geometry and different conditions predefined by the user, such as mesh windows. It also allows to automatically remesh when the elements are distorted in a certain percentage or predetermined value.

For this simulation, around 50000 elements are required, giving good results without making the computing times too long. After trying different number of elements, it is concluded that the Automatic Mesh Generator adjust the number of elements (and the elements themselves) to the predefined conditions, creating around 1/3 of the total elements required. That's why the program was set to create a mesh with 150000 elements:

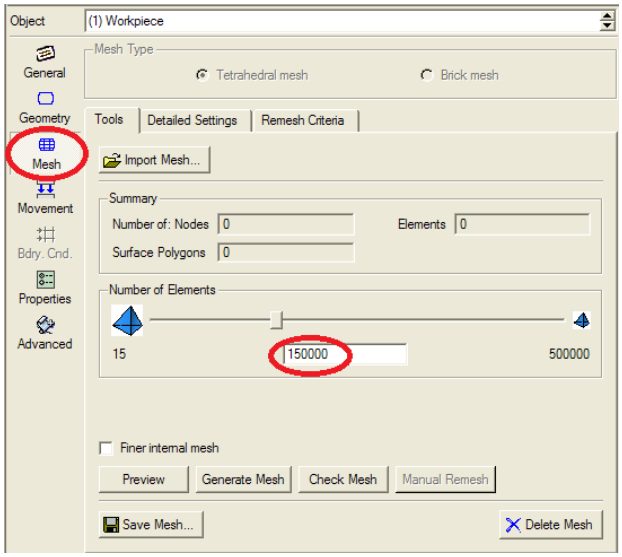

Figure 2.15 *Sheet meshing*

DEFORM™-3D allows to choose between two types of elements: *brick*, with 8 nodes and *tetrahedral*, with 4 nodes. However, once the elasto-plastic option is chosen, it is only allowed the tetrahedral ones.

Given the final geometry of the sheet, it is necessary to refine the mesh in the areas close to the centre of the piece. For that, *detailed settings* must be clicked, where it can be configured. First the weighting factors have to be adjusted, making the *mesh density window* the main one, giving it a value of 1.

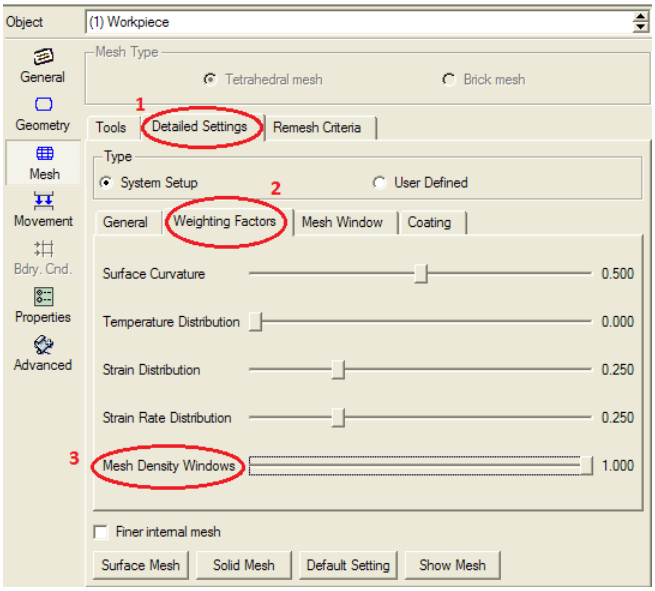

Figure 2.16 *Detailed meshing settings*

After that, mesh windows will be created. In this case, 2 different mesh windows were set: the inner one with a size ratio of 0.12 (being the most deformed part, a thinner mesh is needed), and the outer one with a size ratio of 0.25. That sizes, along with the number of elements have proven to be enough to provide good results, without long computing times.

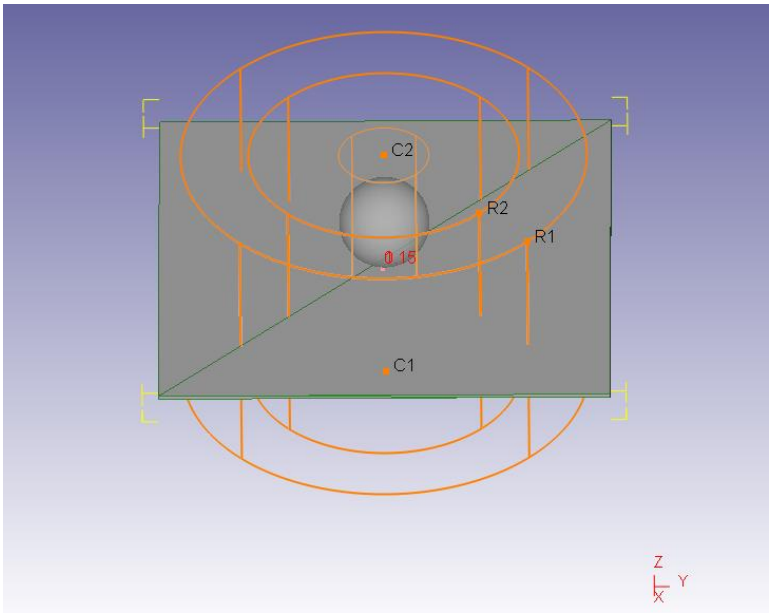

Figure 2.17 *Different meshing windows*

Now the only thing remaining is simply clicking the Generate Mesh button on the main meshing window (*Figure 2.15*). It must be noted that DEFORM™-3D sometimes has a problem with the meshing, where despite having given the program different mesh windows, it doesn't use them, generating an uniform mesh:

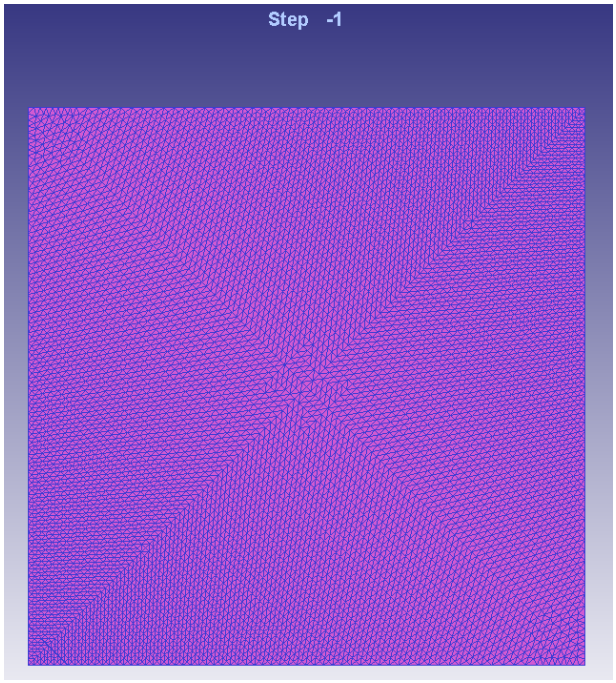

Figure 2.18 *Problem with the meshing*

This has a very simple solution: the simulation setting will continue with this mesh, and after the work with the pre-processor is finished, the program will be set to run a few steps, stopping the program after that, and manually remesh again in the pre-processor (as the mesh windows are already defined, it is enough with just clicking the generate mesh button). With that done, the meshing result is as follows:

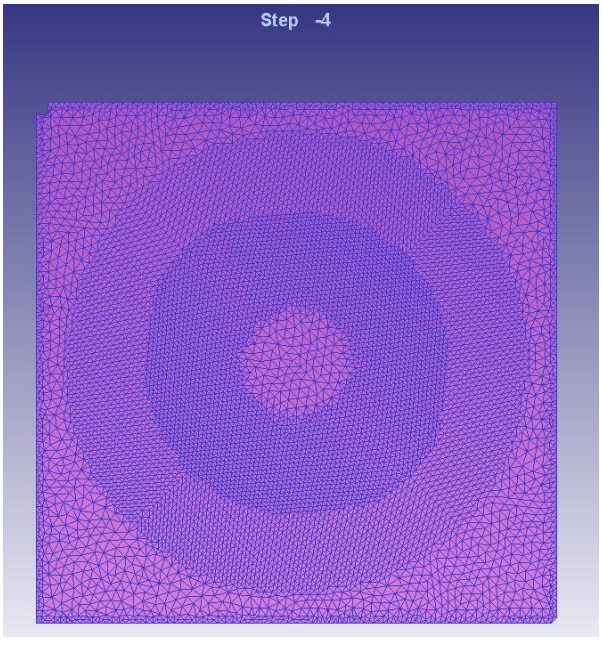

Figure 2.19 *Final meshing for the 20mm tool*

As it can be seen, with the remeshig, DEFORM™-3D often loses some material from the geometry. In this study it isn't considered, as they are minimal loses, and they are located away from the studied zone. Sometimes during the simulation, the mesh were too much distorted, generating folding problems and being necessary to stop the simulation, and to remesh manually as it was explained before. In those cases, the new start point of the simulation was set at a previous step before the occurrence of the above mentioned issue.

With the mesh created, the boundary conditions on the sheet can be set. As told before, this model does not have a blank holder piece, therefore a substitute boundary condition is needed. That's because with the blank holder piece, when the simulation has achieved a noticeable depth, due to numeric errors, part of the sheet gets inside the blank holder (*Figure 2.20*), creating contact problems and invalidating the strain and stress values from that point.

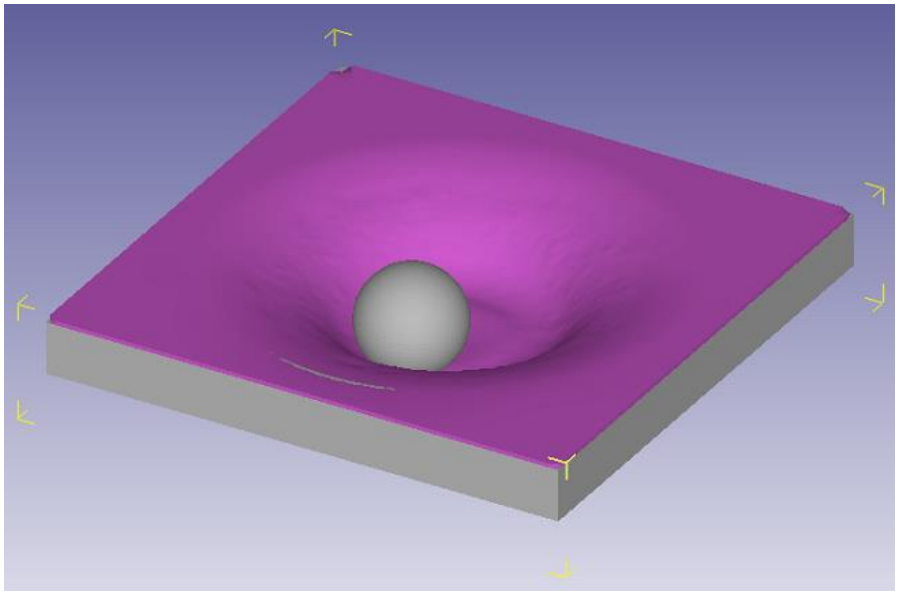

Figure 2.20 *Simulation failure with the blank holder*

To adjust the model to the experimental analysis, different boundary conditions will be set to embed the vertical planes of the sheet, and constraint the vertical movement of the sheet there where the blank holder would be.

For that, the *Bdry. Cnd.* tab must be clicked, and set three different boundary conditions, one on each axis (x, y, and z). For that, it will be used the velocity condition, setting it to a value of 0. For the x, y directions, it's only needed to set the condition on the nodes of the vertical planes. For the vertical direction, a similar tool as when setting the mesh windows will be used. In this case, it will be set with an outer radius enough to cover the entire sheet, and an inner radius of 42mm. That value is to adapt the condition of the experimental blank holder, which had an inner radius of 40mm, and a 2mm rounded edge. This solution, although it can't exactly describe the movement around the blank holder, gives good enough results.

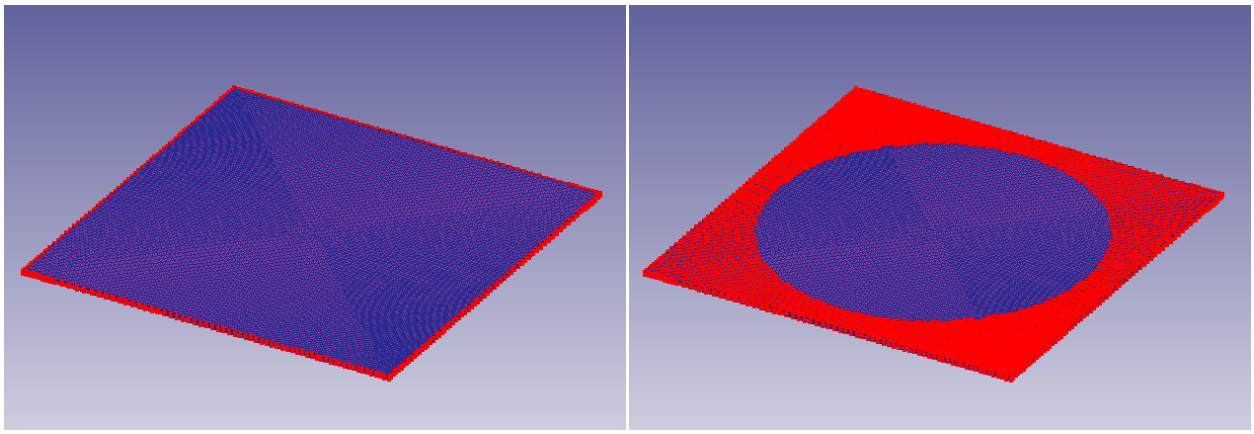

(a) (b)

Figure 2.21 *Boundary conditions in x and y directions* (a) *and in z direction* (b)

Now the movement of the tool will be set. As said previously, in SPIF processes, the tool moves along a trajectory generated in a CNC machine, incrementally forming the sheet to achieve the final geometry. Given the fact that our main goal is to compare the results of this simulation with the experimental, the simulation parameters will be the same from the experimentation.

However, there is a difference, because the tool doesn't rotate on itself. The rest of the parameters are indeed equal, setting the feed rate of 3000mm/min, and a step down of 0.5mm. This step down is used in 2.5 axis CNC machines that are only capable of interpolate trajectories in one of the 3 main planes (being in this case the horizontal one), and make linear movements in the remaining axis. If there is a complex geometry, it will be discretized in several planes. If the machine was 3-axial, the trajectory would describe a 3-dimensional geometry, without discretization in planes.

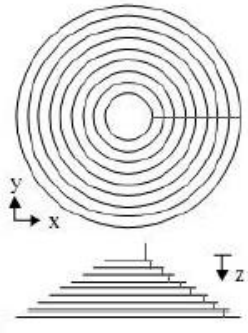

Figure 2.22 *Tool trajectory with the step down*

In order to create the points of the trajectory, PHYTON™ interface was used, that generated all the points where the tool would move, after introducing the step down, the tool radius, the feed rate, if the free rotation of the tool is permitted, the direction of rotation (-1 if constant, 1 if alternate, that was our case), and if there is a pyramidal or conical geometry.

To introduce that trajectory in DEFORM™-3D, the tool will be selected in the object tree, and in the movement tab, the *Path* option will be selected. Given that the feed rate is known, as also the points of the trajectory, the function will be defined as *Profile+feed rate*:

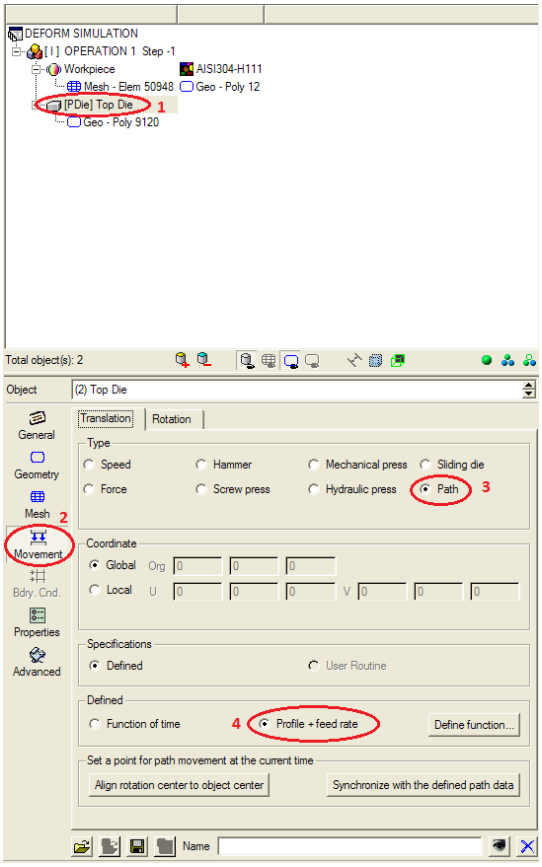

Figure 2.23 *Movement window in the pre-processor*

After that, it's needed to click in define function and introduce the x, y, z coordinates of all the points, and the feed rate, as a table, to obtain the following:

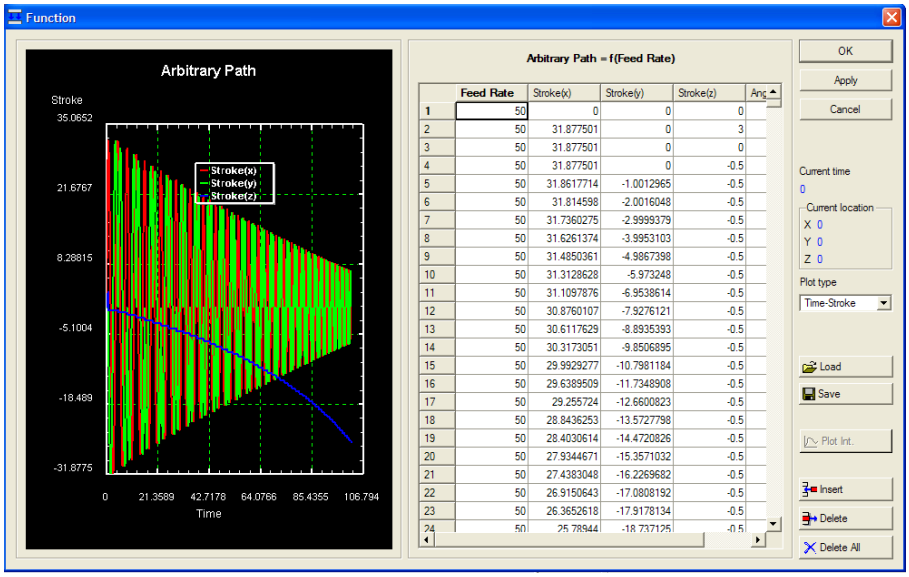

Figure 2.24 *Point cloud of the trajectory*

Now the interactions between the two pieces will be set. For that, the inter object option will be clicked on the main toolbar:

Figure 2.25 *Main toolbar on the pre-processor*

In the window that will open, the master and slave pieces must be selected. In this case, the sheet is formed by the tool, so the tool is the master and the sheet the slave. The friction value is introduced here, value that was estimated of 0.01 of Coulomb friction, that suits better the condition on a lubricated forming such as ours.

Sometimes, despite creating the interaction, the program has problems obtaining the contact conditions. That problem doesn't affect the simulation, because when the tool starts forming the sheet (some steps after the beginning of the simulation), it is correctly detected.

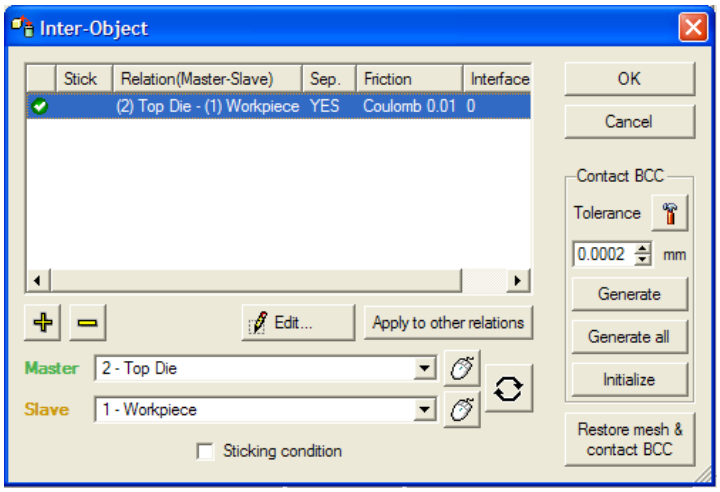

Figure 2.26 *Inter object and friction window*

To finish with the pre-processor, the simulation parameters will be set in *Simulation Controls*. As said before, units are in SI (being length in mm and the stresses in MPa).

In order to calculate the approximate number of steps necessaries for the simulation, the real time of the process was divided by the step increment control (that was set of 0.005sec/stem), obtaining around 22000 steps. Choosing a right number of steps is very important, because that's what DEFORM™-3D uses to calculate. If too few steps are chosen, the simulation may end before the tool finishes forming the workpiece.

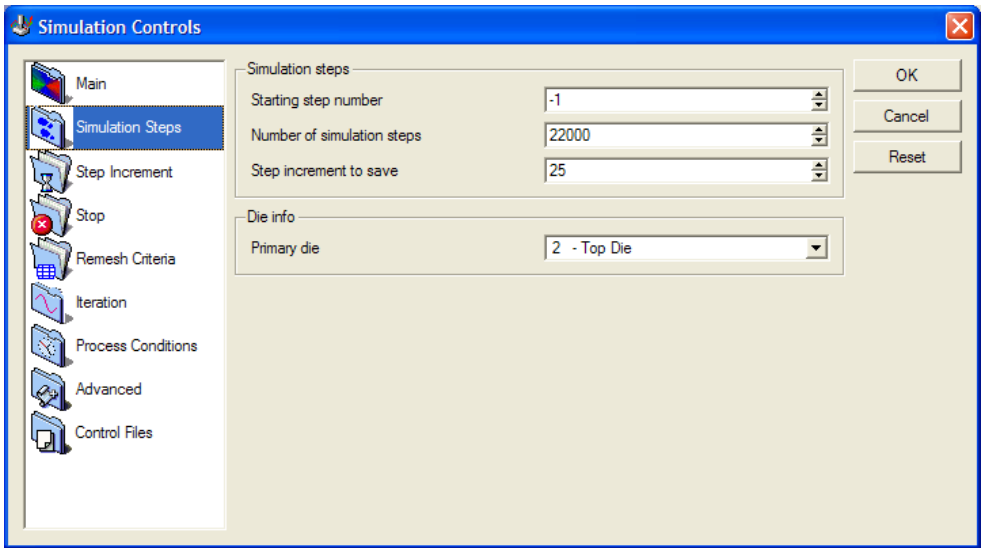

Figure 2.27 *Step number selection*

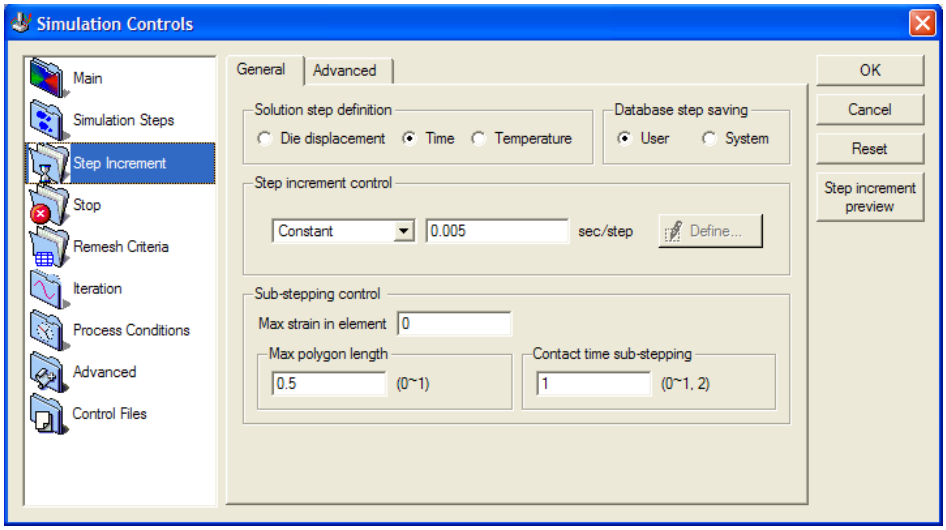

Figure 2.28 *Step increment control number selection*

With all set, and before starting the simulation, it is needed to check and generate an initial database:

Figure 2.29 *Main toolbar on the pre-processor*

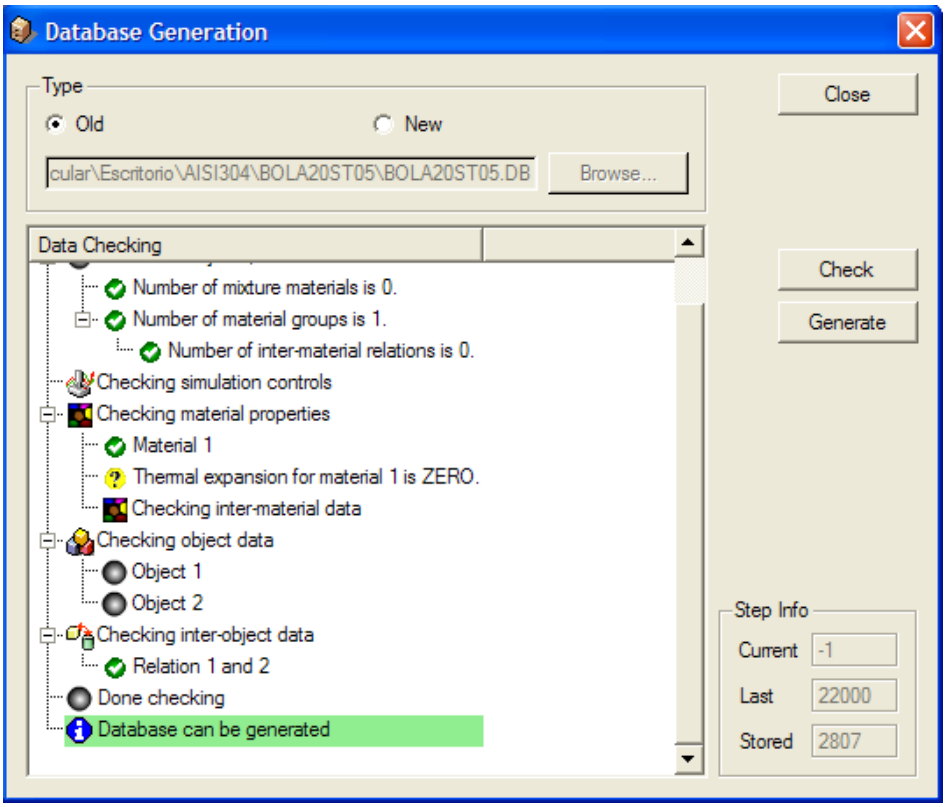

Figure 2.30 *Database checking and generation*

Once the database is generated, the *pre-processor* can be closed and start the simulation by clicking in the *run* button.

DEFORM™-3D has an option of controlling the forming process during the simulation, allowing to modify it in the middle, or starting again as long as there isn't a conceptual error, such as a wrong introduced data.

Now, it will be shown the analysis of results obtained at real failure depths: 24.5 mm for the 20 mm tool, and 28 mm for the 10 mm tool.

3 RESULTS

With the DEFORM™-3D numeric tool, it was possible to predict the material flux, in both cases, with the 20 and 10 mm diameter tools.

As said before, the main objective on this project is to validate the model in terms of strains, comparing them with the experimental processes. The principal strains analysis will consist in the search of the values distribution, and the locations where they are higher. It will be done just in the instant in which the tool displacement reaches vertically the experimental failure depth.

3.1 20 mm diameter tool

The numeric results bear out the experimental ones. The major strain ε_1, is inside the obtained values, with zones in which its value is around 0.9, as shown in *Figure 3.1* in the red shaded areas. As can be seen, those areas are placed in the higher displacement areas, being there where the fracture would locate.

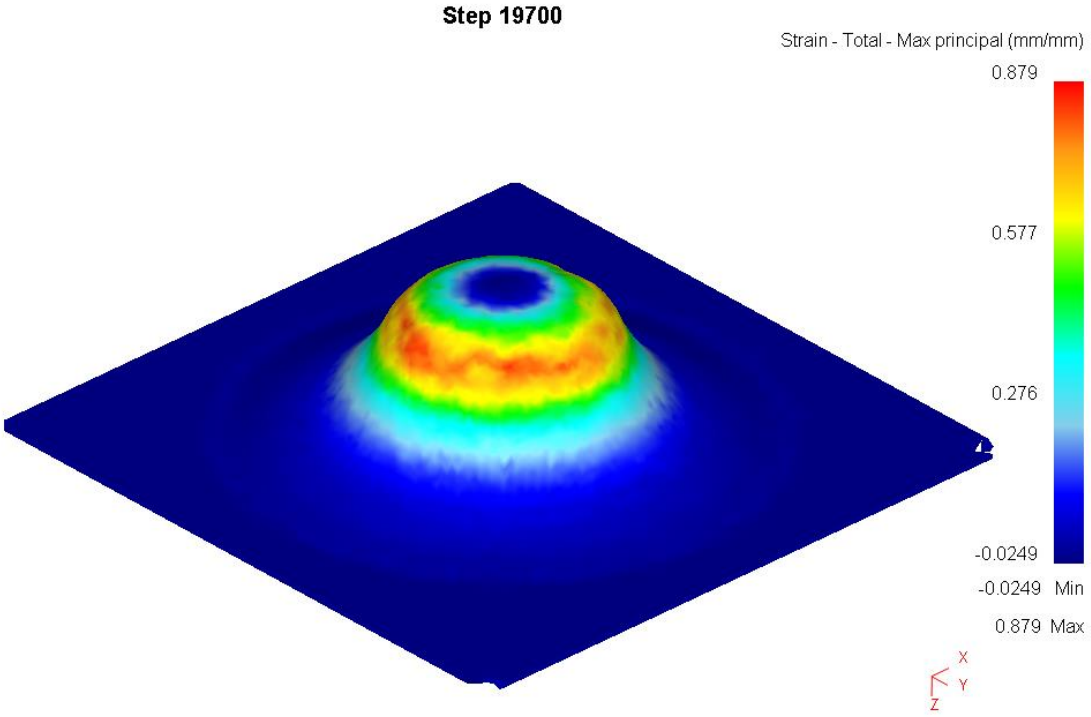

Figure 3.1 *Mayor strain distribution in the outer surface of a SPIF formed AISI304 sheet with a 20 mm diameter tool*

If a dot line is set in the outer surface of the sheet, the following strain curve is obtained. The position of the line was arbitrarily set on the origin YZ plane, and that's why the results doesn't reach the maximum value of $\varepsilon_1 = 0.842$ obtained in the fracture points.

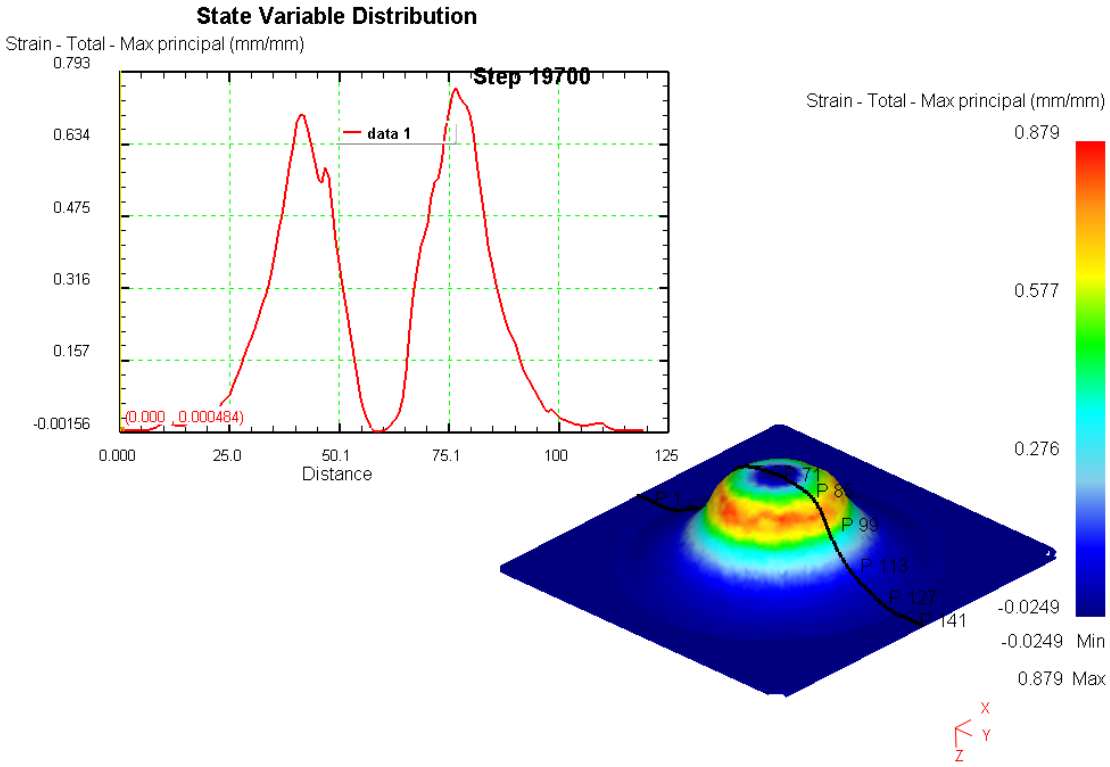

Figure 3.2 *Mayor strain distribution along a dot line in the outer surface of a SPIF formed AISI304 sheet with a 20 mm diameter tool*

Regarding the minor strain, ε_2, it can be seen that its value remains between 0.15 and 0.2 in the formed zone, that matches the experimental results. However, it can be seen a zone where its value rises to around 0.8, specifically the area where the forming tool executes the step down. That doesn't correspond with the experimentation, and it's probably due to numeric errors during each step down. Since experimentation shows that the fracture doesn't occur in that area, we will obviate the results on the step down zone.

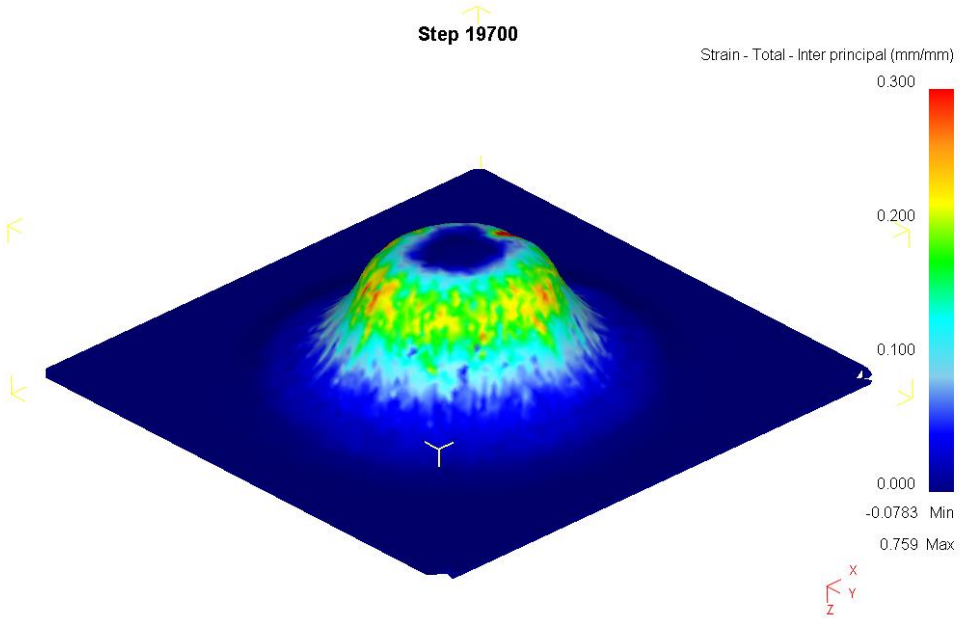

Figure 3.3 *Minor strain distribution in the outer surface of a SPIF formed AISI304 sheet with a 20 mm diameter tool*

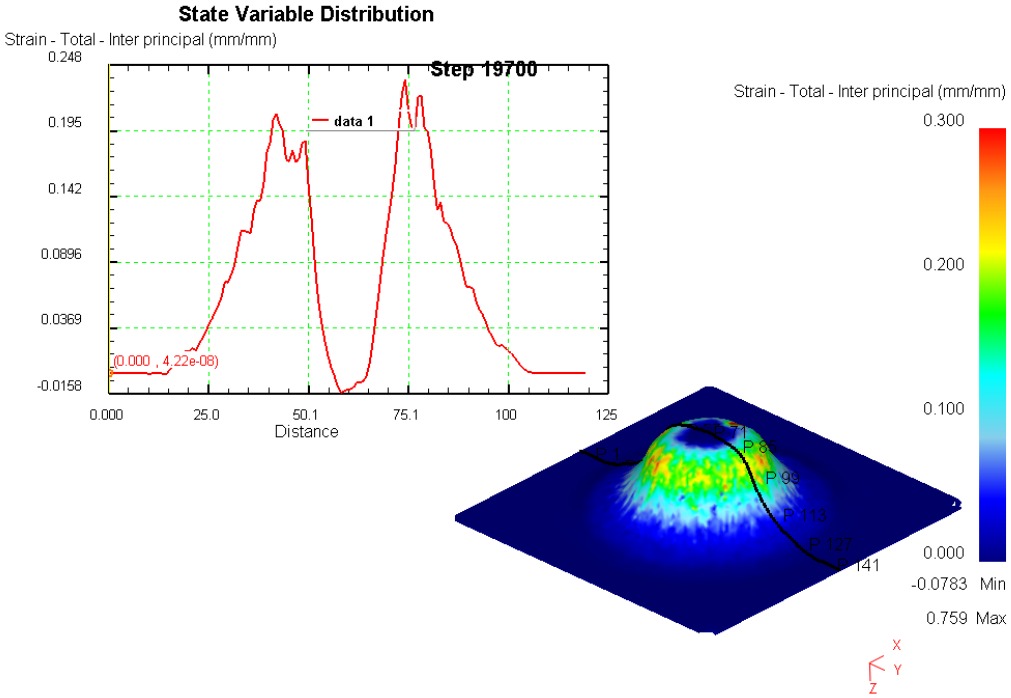

Figure 3.4 *Minor strain distribution along a dot line in the outer surface of a SPIF formed AISI304 sheet with a 20 mm diameter tool*

To compare the experimental results, and the numeric ones obtained in DEFORM™-3D, they will be represented together in the same graph, as follows:

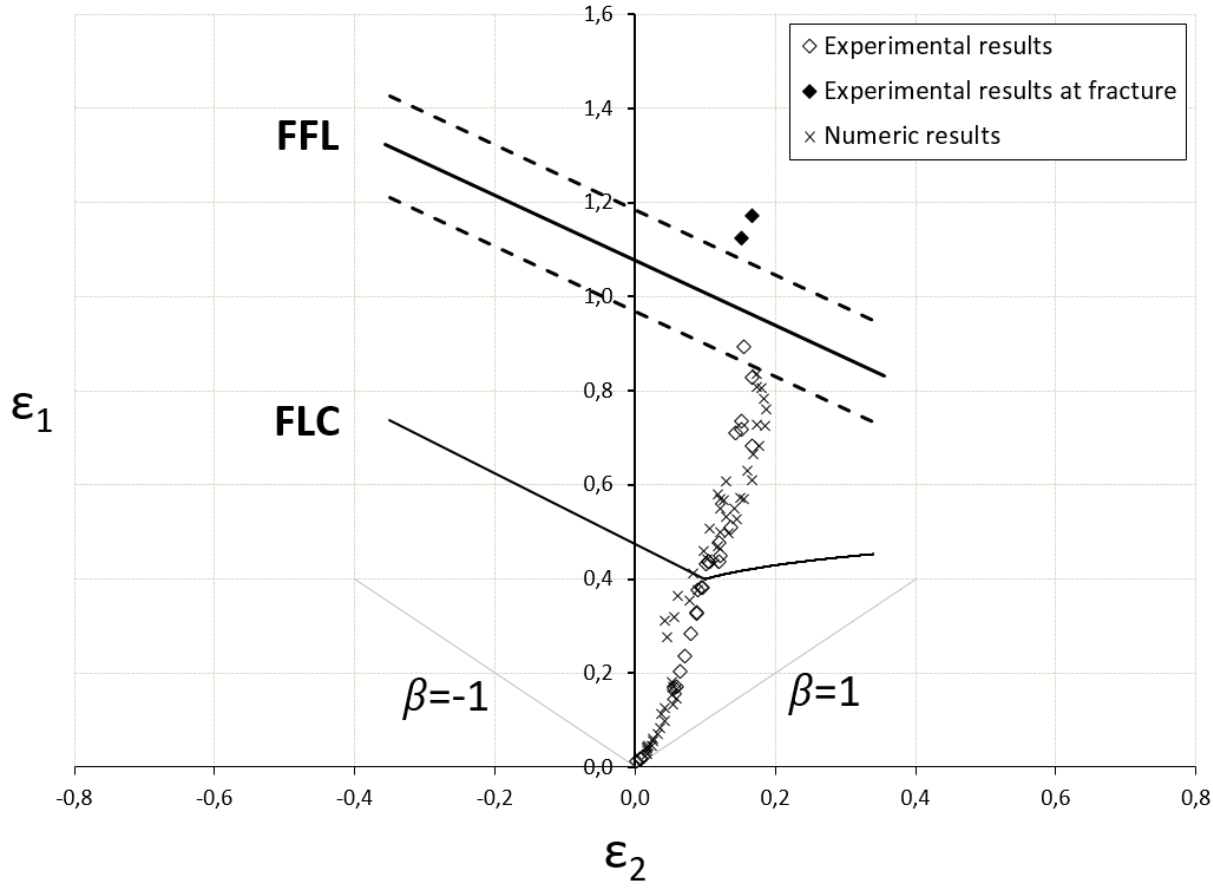

Figure 3.5 *Experimental and numeric results of the formability until fracture of a SPIF formed AISI304 sheet with a 20 mm diameter tool*

The numeric points in the graph have been obtained by selecting points from several dot lines as the one shown in *Figure 3.2* and *Figure 3.4*, each line with a different orientation in order to get points from all the geometry. It can be seen that the results from the simulation resemble the experimental ones almost exactly, although some points are slightly displaced to the left under the FLC curve. Regardless this small distortion from the experimental results, the numeric ones accomplish stable plastic deformation above the FLC curve, following the experimental analysis.

Notice that in the simulation, the mayor strain doesn't reach the experimental fracture values. That's because in the experimental process a necking appeared, increasing the value of the major strain. Since DEFORM™-3D can't predict the necking development, its results only adapt the pre-necking experimental results.

Since several remesh steps were needed in order to complete the simulation, it's worth to evaluate the evolution of some parameters in each remesh, such as the mesh volume, and the computing time required. The simulation was performed on a computer with Windows XP, and Intel® i7 920 processor working with 1 core. Results are shown in *Table 3-1*:

Table 3-1 *Parameters of interest during different remeshings*

Mesh	Total number of elements	Total steps performed	Simulation time between meshings (approx.)	Mesh volume (mm^3)	% volume variation from initial
Initial mesh	50872	3	<1 min	8000.05	0
Remeshing 1	54206	17000	72 hrs	7993.72	-0.07912451
Remeshing 2	46992	19200	10 hrs	8147.54	1.84361348
Remeshing 3	44033	19375	1 hr	8187.91	2.34823532
Remeshing 4	43768	19400	10 min	8184.63	2.30723558
Remeshing 5	44651	19605	1 hr	8182.38	2.27911076
Remeshing 6	44842	19700	30 min	8179.74	2.24611096

As shown in the table, as the simulation goes further, more frequent remeshings are needed. That's because of the final frustum geometry, meaning that the deeper the tool is, the faster it deepens, because the curve gets smaller in each step down, distorting the mesh faster.

The simulation time is highly estimated, firstly because of the impossibility of the author of this project to be always controlling the simulation, and secondly because in order to realize the necessity of a remeshing, it was needed the simulation to run some steps more, to notice the failure, and then remesh several steps before the failure (in this project, the remeshings were done about 100 steps before the failure step every time it was possible), roughly extending the total simulation time (from the initial meshing to the end of the simulation) to 5 days or a week.

As can be seen, the mesh volume slightly increases during the simulation. This is due to numeric errors in the nodes of the mesh, but since the total variation is smaller than a 5%, it isn't considered.

3.2 10 mm diameter tool

The process with the 10 mm diameter tool presents a slightly worse geometry, caused by numerical errors because of the indentation of the tool. This means that DEFORM™-3D can't predict the material flux in the 10 mm tool process as well as in the 20 mm one. However, the obtained results in both cases still are acceptable.

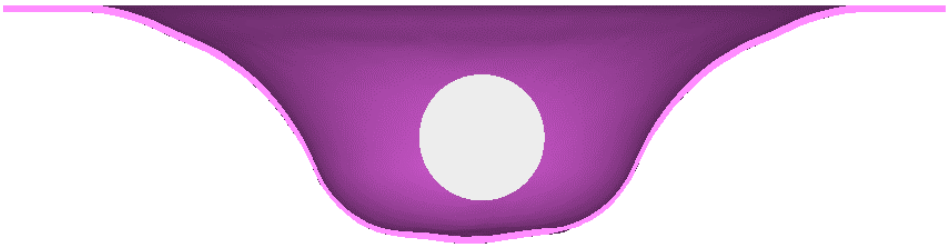

Figure 3.6 *Final geometry of a SPIF formed AISI304 sheet with a 20 mm diameter tool*

Figure 3.7 *Final geometry of a SPIF formed AISI304 sheet with a 10 mm diameter tool*

In this case the same procedure will be used, analysing each strain separately, to finally create the FLD graph with both the experimental and numerical results. Again, the numeric results adjust with the experimental analysis, with a highest value of the major strain of $\varepsilon_1 = 1.28$, located again in the higher displacement areas.

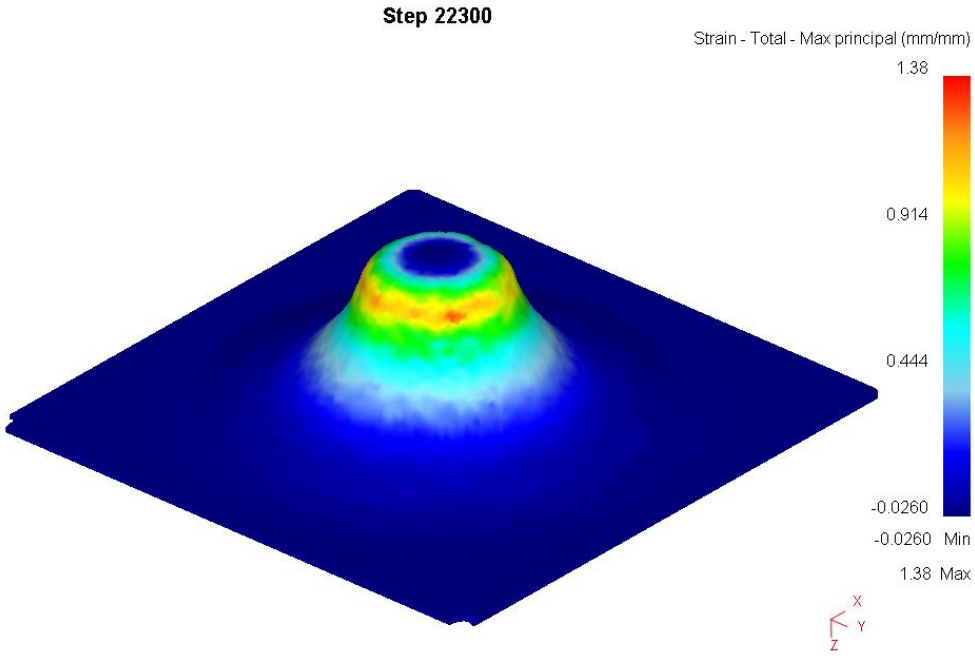

Figure 3.8 *Mayor strain distribution in the outer surface of a SPIF formed AISI304 sheet with a 10 mm diameter tool*

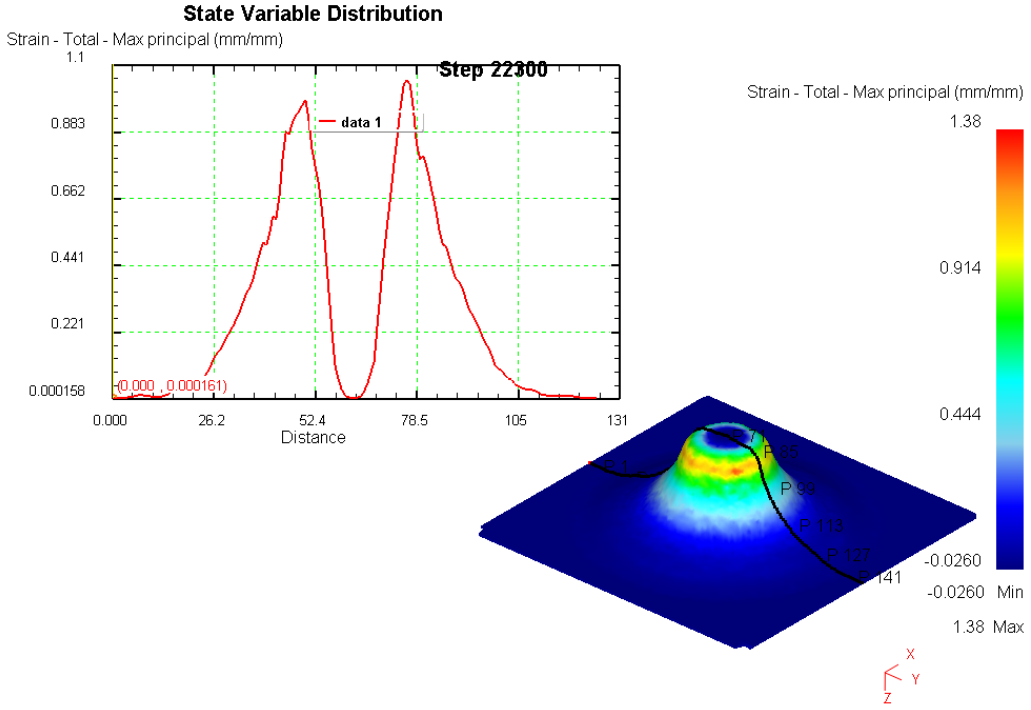

Figure 3.9 *Mayor strain distribution along a dot line in the outer surface of a SPIF formed AISI304 sheet with a 10 mm diameter tool*

Again, the minor strain values correspond with the experimental results in all the geometry but the step down area, which again has values of about 0.7 due to numeric errors, which will be obviated.

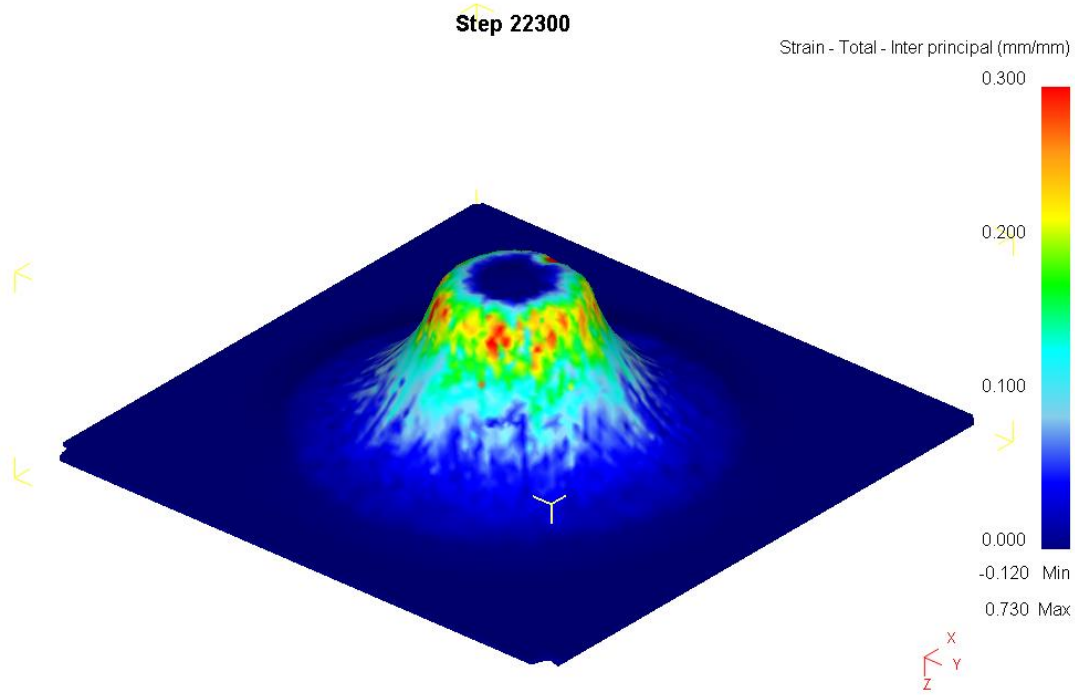

Figure 3.10 *Minor strain distribution in the outer surface of a SPIF formed AISI304 sheet with a 10 mm diameter tool*

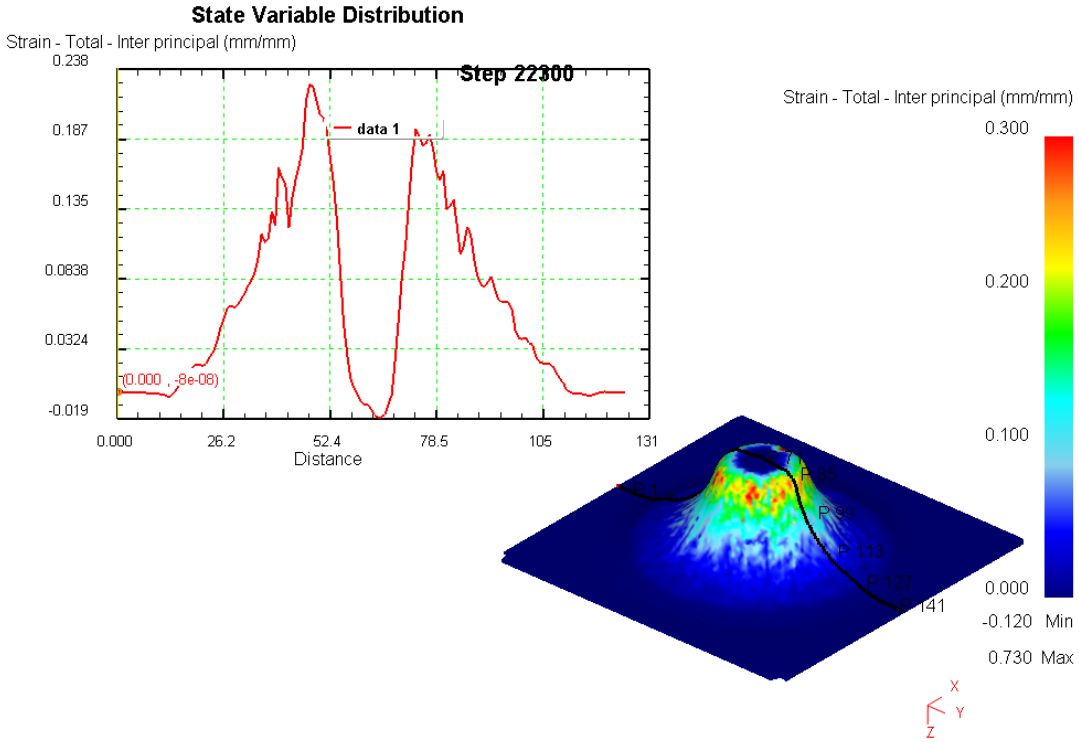

Figure 3.11 *Minor strain distribution along a dot line in the outer surface of a SPIF formed AISI304 sheet with a 10 mm diameter tool*

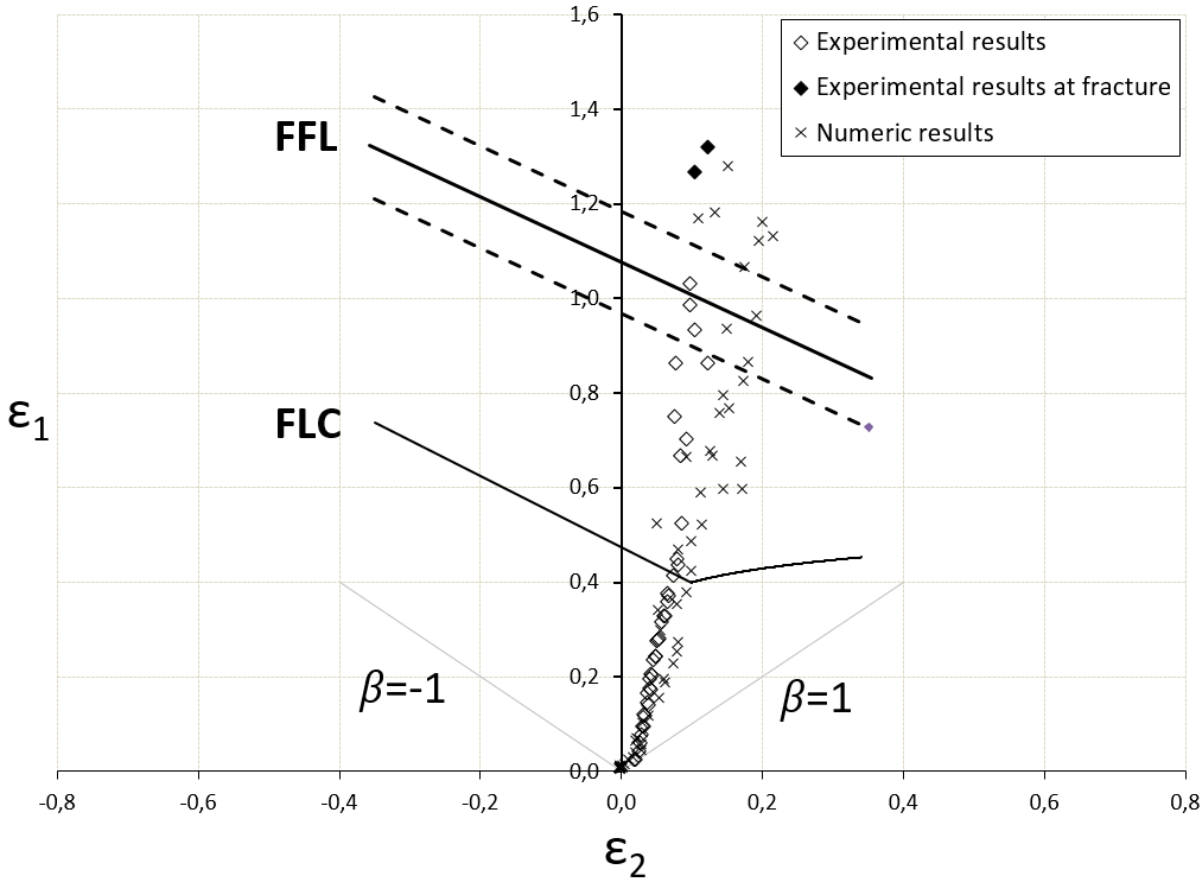

Figure 3.12 *Experimental and numeric results of the formability until fracture of a SPIF formed AISI304 sheet with a 10 mm diameter tool*

Again, representing the experimental and the numeric results in the same graph, allows to compare them. Similar to the 20 mm tool case, here can be seen that the results from the simulation resemble the experimental ones, being slightly displaced to the right.

Since the experimental analysis of the 10 mm tool process proved that there were a much smaller necking within the failure of the sheet than in the 20 mm tool process, in this case the simulation can adjust and predict almost perfectly the final failure strains. That, allows again stable plastic deformation above the FLC curve, and specifically in this case, allowing the principal strains to reach and slightly overpass the FFL curve within stable deformation.

3.3 Accumulated damage

In metal forming it's basic to prevent the fracture failure, depending for that of a strain limit study, as the one that has been realised in this project. By calculating the accumulated damage, it will be possible to calculate when and where the fracture will appear, with the calculated strains and stresses.

DEFORM™-3D uses the Normalized Crockroft & Latham as default damage model, but allows to choose between other damage models, listed here:

- Normalized C&L
- Cockroft & Latham
- McClintock
- Freudenthal
- Rice & Tracy
- Oyane
- Oyane (negative)
- Ayada
- Ayada (negative)
- Osakada
- Brozzo
- Zhoa &Kuhn
- Maximum principal stress / ultimate tensile strength
- User routine

In this project, the Ayada damage model was used:

$$D = \int_0^{\bar{\varepsilon}_f} \frac{\sigma_H}{\bar{\sigma}} \mathrm{d}\bar{\varepsilon}$$

Where D is the accumulated damage, $\bar{\varepsilon}$ and $\bar{\sigma}$ are equivalent strains and stresses, σ_H the hydrostatic stresses and σ_1 the major principal stress. When introducing any damage model in DEFORM™-3D, a critical value is needed, that will be calculated later.

According to fracture mechanics, fracture failure on metal forming has 3 different modes of fracture. The ductile fracture criterion used in this project is based in Mode I.

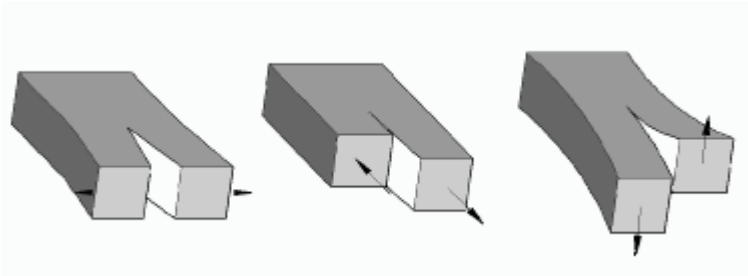

Figure 3.13 *Fracture modes; respectively, Mode I, Mode II, and Mode III*

The circumstances where each fracture mode occurs are identified in terms of microstructural ductile damage and plastic flux. In SPIF, the plastic material flux and the failure is a combination of modes I and II, while in traditional forming methods it's a combination of modes I and III.

With analytic calculus, it's possible to characterize the fracture mode in terms of stress conditions. To study it, Atkins & Mai (1985) established a relationship among the inclusions space, the holes diameter and the triaxial stress state at the onset of the crack propagation.

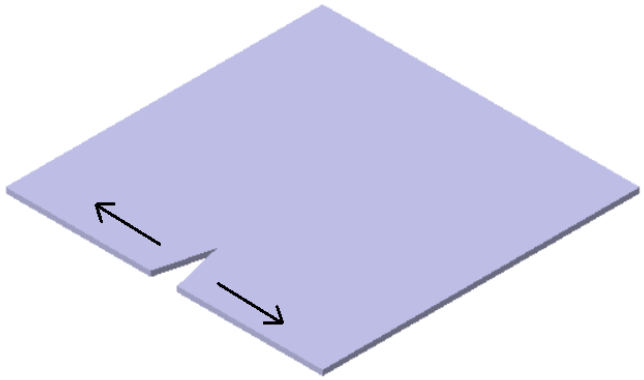

Figure 3.14 *Crack propagation in fracture Mode I*

Results of the analysis, proved that the critical damage was as follows:

$$D_{crit} = \int_0^{\bar{\varepsilon}} \frac{\sigma_H}{\bar{\sigma}} \, \mathrm{d}\bar{\varepsilon}$$

That equation, developed under Hill's anisotropic plasticity criterion, with plane stress conditions, gives, as exposed on Silva et al (2008-09-11):

$$D_{crit} = \frac{(1+r)}{3}\left(\varepsilon_{1f} + \varepsilon_{2f}\right)$$

As in this project it has been assumed the isotropy of the material, r is determined and equal to 1; and ε_{1f} and ε_{2f} are respectively the mayor and minor strains on the fracture point. This allows to conclude that the tensile fracture limit in Mode I is independent of the strain path and equivalent to the critical thickness reduction.

Therefore, with this results it's possible to check if the accumulated damage in the simulation corresponds the critical damage obtained in the experimentation, when ductile fracture appears. The integral equation will be used to calculate the accumulated damage on the simulation until experimental failure strains are reached, and the discrete one will allow to obtain the critical damage with the values of r and the mayor and minor fracture strains of the experimental tests.

Thus, it will be possible to predict if the simulation reached the critical damage, knowing that the area where it is reached will be where the fracture would occur. That doesn't mean that it will always happen in the same point, but it bears out if it will happen when the experimental depth is reached.

With the strains results obtained by Centeno et al (2014), the experimental critical damage values are:

Table 3-2 *Strain fracture and experimental critical damage values*

	ε_{1f}	ε_{2f}	$D_{crit} = \frac{2}{3}(\varepsilon_{1f} + \varepsilon_{2f})$
20 mm diameter tool	0.95	0.15	0.733
10 mm diameter tool	1.1	0.1	0.8

3.3.1 20 mm diameter tool

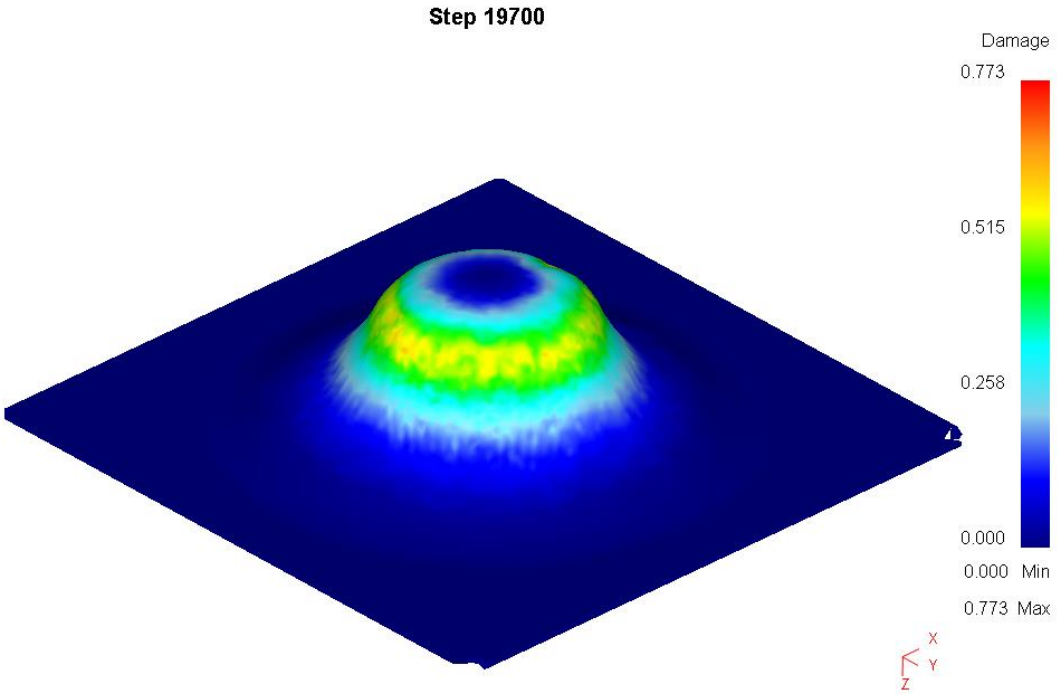

Figure 3.15 *Distribution of the accumulated damage according the Ayada criterion on a SPIF formed AISI304 sheet with a 20 mm diameter tool*

As can be seen, although in the simulation the accumulated damage is slightly higher than the experimental one, it fits quite well in areas of maximum mayor strain, being most of those areas with values around 0.5, and some punctual zones where it reaches the critical value (small orange/red dots).

3.3.2 10 mm diameter tool

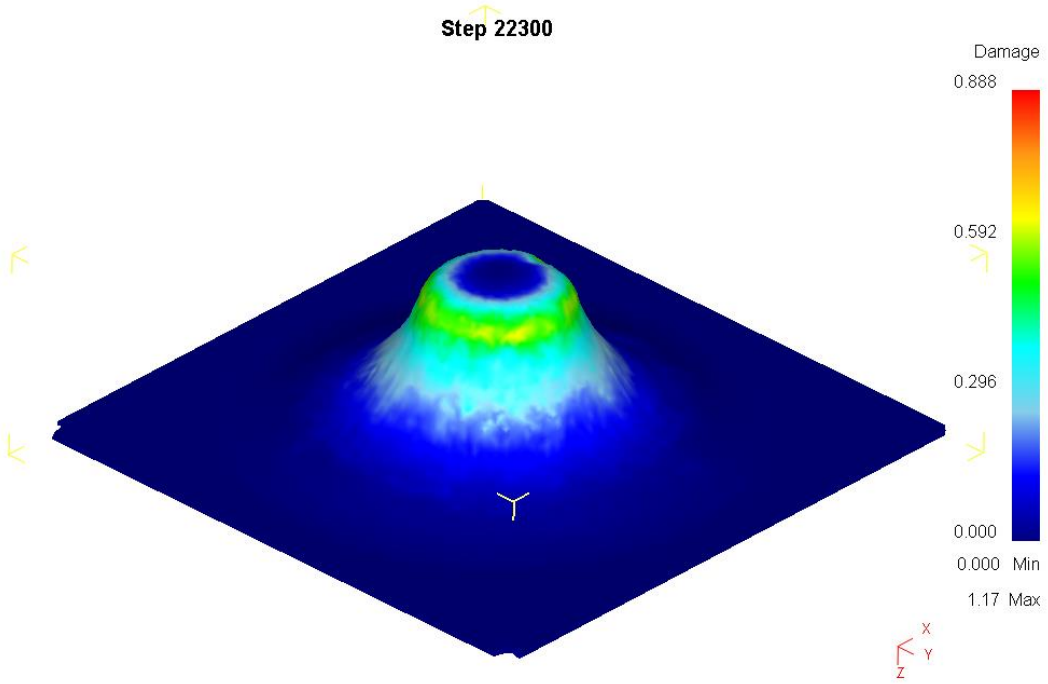

Figure 3.16 *Distribution of the accumulated damage according the Ayada criterion on a SPIF formed AISI304 sheet with a 10 mm diameter tool*

Similar to the 20 mm tool diameter case, the accumulated damage is slightly higher in this simulation than the experimental critical damage, fitting the experimental results with acceptable accuracy in areas of maximum mayor strain.

4 CONCLUSIONS AND FUTURE DEVELOPMENTS

4.1 Conclusions

In this project was created a Finite Element Method model in DEFORM™-3D, for 0.8 mm thickness AISI304-H111 sheets, in order to analyse the strain state during the process. After comparing the simulation results with the experimental ones obtained by Centeno et al. (2014), it was proved that they fit quite well to the experimentation, allowing to validate the numeric model.

Because of the long computing times, several simplifying assumptions were made in the model, such as considering the material as isotropic, and setting the boundary conditions as embeddings in the vertical planes of the sheet. Although it wasn't to reduce the computing time, it's worthy to mention the vertical condition that replaces the blank holder to solve the numeric problems commented.

Those simplifications might affect the small differences between the numeric and the experimental results, but they were done to reduce computing times, but still provide results that followed acceptably the ones from the real process.

Thus, the simulations where accomplished, following the same parameters as the experimental tests. There were performed with 20 mm and 10 mm diameter tools, and the step down was set to 0.5 mm. Therefore, not all the experimental tests where simulated (since in the experimentation, tests were performed with 0.2 mm step down, too), but given that the results for each step down proved to be very similar, it wasn't necessary. In both simulations, the principal strain levels at the real failure depth where similar to the experimental ones. Principal strains from the simulations were compared with the experimental results in the Forming Limit Diagram, for each case.

Critical damage levels were also analysed, comparing the critical damage obtained in the experimentation with the values provided by the Ayada criterion in the simulation, at the real failure depth. In both cases, 10 mm and 20 mm diameter tools, the obtained values were very close to the experimental, proving that the Ayada criterion allows to properly predict plastic failure in this simulations.

Finally, with the simulations concluded and analysed, a step by step manual was created to easily show how to model the incremental forming processes carried out in this project, using DEFORM™-3D.

4.2 Future developments

Once the model is validated, it could be extrapolated to other tool diameters, such as 8 mm, 12 mm, etc., or trying to determine the smallest diameter for which DEFORM™-3D can't correctly predict the material flux. Other parameters could be numerically analysed, such as the influence of the feed rate, the friction, the tool rotation or the element size, creating different meshes, or variating the mesh size on the remeshes.

Another Finite Element Method softwares could be used, implementing models in both explicit calculation based models such as LS-Dyna®, and implicit ones as Abaqus®, to be able to compare which program gives better results in simulated SPIF processes.

Finally, it could also be extended to other industrial application variants of SPIF with different geometries, such as hole flanging processes.

REFERENCES

Amino, H. et al., 2002. Dieless NC Forming, Prototype of automotive Servive Parts *Proceedings of the 2nd International Conference on Rapid Prototyping and Manufacturing (ICRPM).*

Aoyama, S., Amino, H., Lu Y. & Matsubara, S., 2000. *Apparatus for dieless forming plate materials.* Europe, Patent No. EP0970764.

Candel, Z. Análisis numérico de la conformabilidad de chapas de AA2024-T3 en procesos de conformado incremental mono-punto usando DEFORM-3D. Trabajo de Fin de Grado. *University of Seville.*

Carmona, J. Numerical Analysis on DEFORM-3D of limit strains in Single Point Incremental Forming for AISI304-H111 sheets. Proyecto de Fin de Carrera. *University of Seville.*

Centeno,G. et al., 2011. *Experimental Study on the Overall Spifability of AISI 304.* Sevilla-Girona, University of Sevilla & University of Girona, p. 8.

Centeno, G. et al., 2012. *FEA of the Bending Effect in the Formability of Metal Sheets via Incremental Forming, Steel Research International.* pp 447-450.

Centeno, G. et al., 2012. Experimental Study on the Evaluation of Necking and Fracture *MESIC,* p.8.

Centeno, G. et al., 2014. Critical analysis of necking and fracture limit strains and forming forces in single-point incremental forming *Materials and design,* Volume 63 pp.20-29.

Emmens W. & Van den Boogaard, A., 2009. An overview of stabilizing deformation mechanism incremental sheet forming, *Journal of Material processing Technology* , Volume 211 pp. 3688-3695.

Goodwin, G., 1968. Application of strain analysis to sheet forming problems in the press shop. *MET ITAL,* Aug, 60(8), pp. 767-774.

Hirt , G., 2004. Tools and Equipment used in Incremental Forming. *Incremental Forming Workshop, University of Saarbruckewn,* June 9. p. 27.

Hirt, G., Ames, J., Bambach, M., & Koop, R., 2004. Forming strategies and Process Modeling for CNC Incremental Sheet Forming. January, Volume 53, p. 203.

ISO, 2008. 12004-2:2008. *Metallic materials -- Sheet and strip -- Determination of forming-limit curves -- Part 2*: *Determination of formig-limit curves in the laboratory*.

Jeswiet, J., Duflou, J., Szekeres, A. & Levebre, P., 2005. Custom Manufacture of a Solar Cooker - a case study. *Journal Advanced Material Research,* May. Volume 6-8.

Jeswiet, J., et al. 2010. *Asymmetry Single Point Incremental Forming of Sheet Metal.*

Keeler, S., 1965. Determination of forming limits in automotive stampings. SHEET METAL IND, Sep, 42(461), pp. 683-691.

Leszak, E., 1967. *Apparatus and Process for Incremental Dieless Forming.,* Patent No. US3342051A1.

Marciniak, Z., Duncan, J. & Hu, S., 2002. *Mechanics of Sheet Metal Forming.* London Butterworth-Heinenrmann.

Meier, H., Dewald, O. & J., Z., 2005. Development of a Robot-Based Sheet Metal Forming Process. *In steel research,* Volume 1.

Powell, N. & Andrew, C., 1992. Incremental forming of flanged sheet metal components without dedicated dies. *IMECHE part B, J. of Engineering Manufacture,* Volume 206.

Ruiz, F. Análisis numérico de procesos de conformado incremental monopunto en chapas de aluminio AA7075-T3. Trabajo de Fin de Grado. *University of Seville.*

Schafer, T. & Schraft, R. D., 2004. Incremental sheet forming by industrial robots using a hammering tool. *AFPR Association Francais de Prototypag Rapid, 10th European Forum on Rapid Prototyping,* 14 Sep.

Schmoeckel, D., 1992. Developments in Automation, Flexibilization and Control of Forming Machinery. *Anuals of CIRPM,* Volume 40/2, p. 615.

Silva, M., Nielsen, P., Bay, N. & Martins, P., 2011. Failure mechanims in single-point incremental forming of metals. 1 March.

Silva, M., Skjoedt, M., Bay, N. & Martins, P. & Bay, N., 2008. Revisiting single-point incremental forming and formability/failure diagrams by means of finite elements and experimentation. *International Journal of Machine Tools & Manufacture,* Issue 48, pp. 73-83.

Silva, M., Skjoedt, M., Martins, P. & Bay, N., 2007. Revisiting the fundamentals of single point incremental forming by means of membrane analysis. *International Journal of Machine Tools & Manufacture,* Issue 48, pp-3-5.

Skjoedt M., Bay N., Endelt B. and Ingarrao G., 2008. Multi-stage strategies for single point incremental forming of a cup. *11th ESAFORM conference on metal forming – ESAFORM2008.*

Stewart, D., 2005. A Platform with Six Degrees of Freedom. *UK Institution of Mechanical Engineers Proceedings,* 180 (15).

Suntaxi, C., 2013. Análisis experimental de deformaciones límite en chapas de acero AISI 304 en conformado incremental. Trabajo de Fin de Máster. Universidad de Sevilla.

Resumen Trabajo Fin de Grado

Ingeniería Aeroespacial

Análisis numérico en DEFORM-3D de deformaciones límite en conformado incremental mono-punto de chapas de acero AISI304-H111

Numerical Analysis on DEFORM-3D of limit strains in Single Point Incremental Forming for AISI304-H111 sheets

Autor: Álvaro Fernández Díaz

Tutor: Gabriel Centeno Báez

Departamento de Ingeniería Mecánica y Fabricación
Escuela Técnica Superior de Ingeniería
Universidad de Sevilla

Sevilla, 2016

1 INTRODUCCIÓN

El conformado de chapas metálicas en la industria actual es un proceso de amplia utilización en un gran número de sectores de producción, estando por tanto en continuo progreso y revisión.

Por ejemplo, en el sector aeronáutico, el estirado de chapa se usa para crear las piezas del fuselaje, siendo necesarios un equipamiento y herramientas muy especializados. Es por esto que esta tecnología solo es rentable a gran escala.

El conformado incremental de chapa (Incremental Sheet Forming, ISF) es un proceso innovador que cumple los requerimientos de flexibilidad, sostenibilidad y coste de las tecnologías de fabricación actuales, en el que no es necesario el uso de maquinaria y equipamiento dedicados, haciendo que sea viable para lotes pequeños y medios.

El conformado incremental mono-punto (Single Point Incremental Forming, SPIF) es el proceso de fabricación más simple entre los basados en el conformado incremental. Consiste en una herramienta hemisférica controlada por una máquina de control numérico (CNC) que sigue progresivamente una trayectoria preestablecida, deformando plásticamente una chapa metálica para obtener distintas geometrías sin necesidad de troquel. Esto permite un aumento en la conformabilidad, además de las otras ventajas mencionadas previamente.

En este proyecto se calculará numéricamente la evolución de deformaciones en una chapa de acero AISI304-H111 para herramientas de 100 mm y 20 mm de diámetro, con un programa basado en el método de los elementos finitos (FEM), el DEFORM™-3D. Esto, bajo ciertas hipótesis, permitirá tener un modelo para comparar los resultados experimentales obtenidos por Centeno et al (2014), así como permitir obtener la evolución de tensiones en la chapa.

1.1 Antecedentes

El aumento de la conformabilidad de chapas metálicas por medio de procesos de conformado incremental, específicamente de conformado incremental mono-punto, ha sido experimentalmente estudiado por varios autores, como Emmens et al (2009), Jeswiet et al (2010) o Silva et al (2011), entre otros.

El grupo de investigación de Ingeniería de los Procesos de Fabricación de la Escuela de Ingeniería de la Universidad de Sevilla del Departamento de Ingeniería Mecánica ha realizado numerosos ensayos

tanto experimentales como simulaciones numéricas sobre el conformado de chapas metálicas sometidas a SPIF, especialmente la influencia de la flexión en los procesos de conformado, evaluando los mecanismos de fallo e investigando qué parámetros les afectan, como hicieron en Centeno et al (2012).

Bajo esa línea de investigación, se ha desarrollado una metodología para obtener los diagramas límite de conformado (Forming Limit Diagram, FLD), tanto para situaciones de estirado como de estirado con flexión. Esta metodología ha sido probada para diversos materiales, como los aluminios AA7075-O, AA2024-T3, o el acero AISI304-H111, entre otros.

Este último material será el que se analizará en este proyecto. En Centeno et al (2014), se obtuvo la siguiente evolución de deformaciones en SPIF, en la cara externa de una chapa de acero AISI304, una vez ocurrió el fallo:

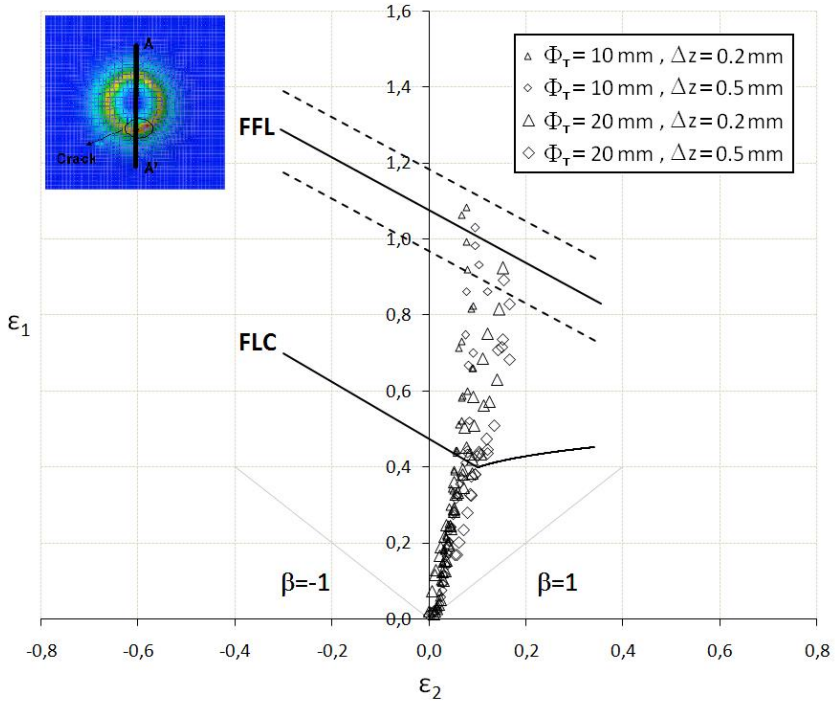

Figura 1.1 *Resultados experimentales para una chapa AISI304-H111 conformada por SPIF con herramientas de 20 mm y 10 mm de diámetro, y steps down de 0.2 mm y 0.5 mm por pasada*

Se llevaron a cabo varios ensayos distintos, con herramientas 6 mm, 10 mm, y 20 mm de diámetro. Para cada herramienta, el step down se ajustó alternativamente a 0.2 mm y 0.5 mm por pasada. Tres ensayos iguales se realizaron para cada uno de los casos, obteniéndose prácticamente los mismos resultados en ellos.

El estado final de deformaciones fue medido con el programa ARGUS®, y las deformaciones de fractura fueron obtenidas midiendo los espesores de la chapa a lo largo de la grieta, a ambos lados de ésta.

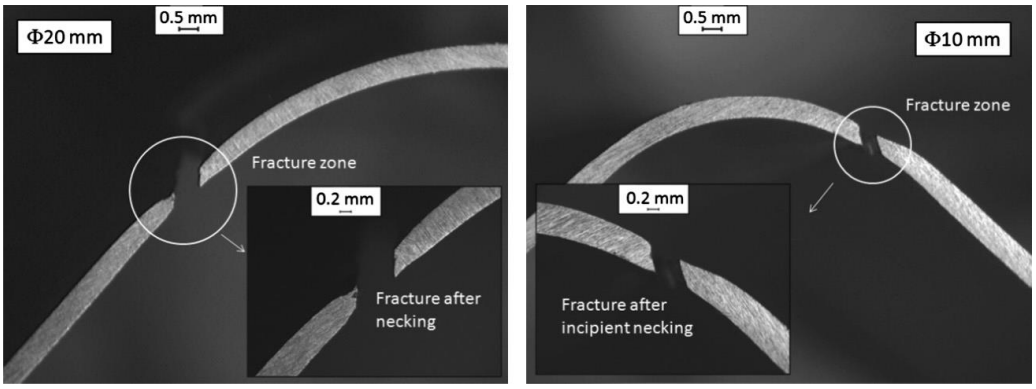

Figura 1.2 *Fractografía de la zona de fallo en el proceso de estirado con flexión (stretch-bending) usando un punzón cilíndrico de 20 mm de diámetro (izquierda), y de 10 mm (derecha).*

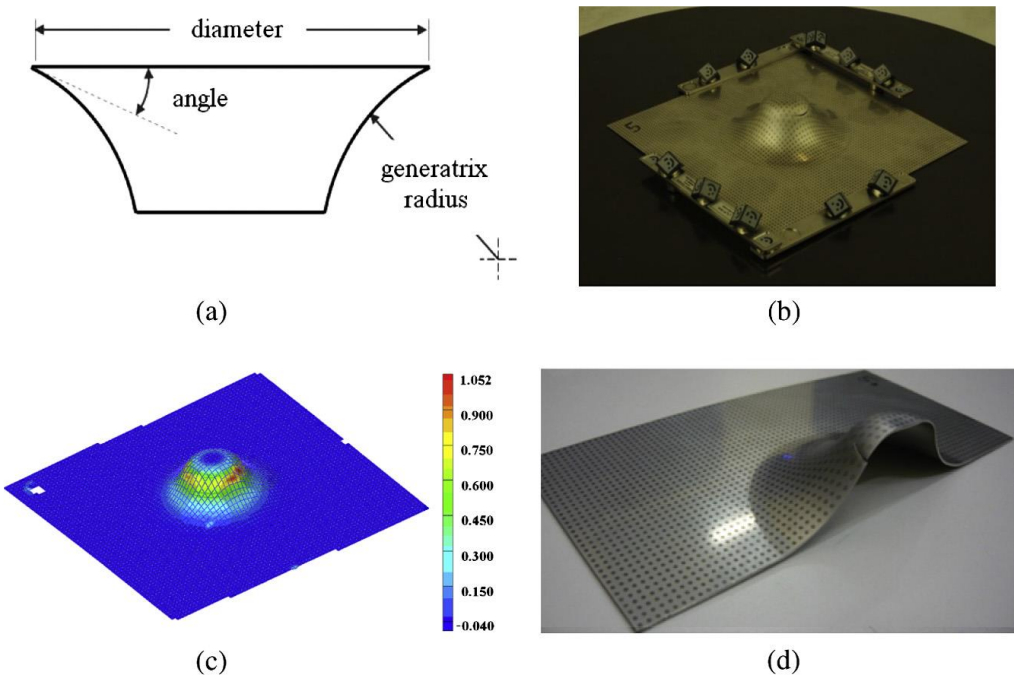

Figura 1.3 (a) *Esquema de la geometría usada en el SPIF,* (b) *patrón de puntos en la geometría final* (c) *resultados de la deformación principal* ε_1 *obtenidos con el programa ARGUS® y* (d) *corte de la geometría final listo para medir los espesores a lo largo de la grieta.*

Como se puede ver en la *Figura 1.1*, hay un gran aumento en la conformabilidad de las chapas de acero AISI304-H111, permitiendo una deformación plástica estable hasta valores de deformación principal ε_1 muy por encima de la curva límite de conformado (Forming Limit Curve, FLC), donde normalmente comienza a haber estricción, y cercanos a la curva de fractura (Fracture Forming Line, FFL). Especialmente, en el caso de la herramienta de 10 mm de diámetro, las deformaciones principales alcanzan la FFL manteniendo una deformación estable. En ese caso, la deformación principal ε_1 alcanza valores de hasta 1.1 en escala logarítmica de deformaciones, ubicándose ligeramente por encima de la curva FFL obtenida en los ensayos de estirado de Nakazima.

2 DEFORM™-3D

En este apartado se comentarán brevemente los pasos clave necesarios para crear el modelo de DEFORM™-3D para los análisis pedidos. Para una guía más detallada, ver el documento original en inglés.

DEFORM™-3D es un sistema procesador de simulaciones que analiza el flujo tridimensional en conformado de metales. Proporciona los flujos de material sin los costes y retrasos derivados del análisis experimental, y ha demostrado ser una solución robusta en el entorno industrial durante más de dos décadas.

DEFORM™-3D permite importar geometrías desde CATIA, y su programa FEM que tiene integrado permite predecir la fractura en múltiples procesos, como mecanizado, estampación, extrusión, laminado, etc.

El generador de malla automático (AMG) genera y optimiza la malla allí donde es necesario. También tiene un sistema *user-defined*, que permite al usuario especificar la densidad de la malla donde convenga. También permite parar la simulación, volver a un paso anterior y modificar los parámetros ahí, permitiendo retomar la simulación desde ese punto. Esta es una de las principales ventajas de DEFORM™-3D en comparación con otros programas FEM, y se utilizará varias veces en este proyecto, ya que a ciertas profundidades la malla se deformará y será necesario remallar manualmente.

2.1 DEFORM™-3D como herramienta numérica

El modelo se creará en el *pre-processor* del programa, siendo necesario primero crear el material y las piezas. Para ello, vamos a la barra principal del *pre-processor*:

Figura 2.1 *Barra principal del* pre-processor, *respectivamente los botones de* Simulation Controls, Material, Object Positioning, Inter Object *y* Database Generation.

En la opción *Material* es posible crear un nuevo material o modificar uno ya existente. En este caso se modificará el existente en la base de datos, con una ley de comportamiento plástico de Norton-Hoff, que permite adaptar la ley de Schwift obtenida por Centeno et al (2014).

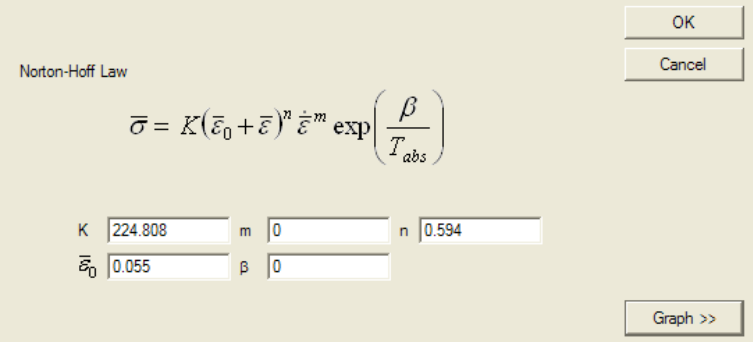

Figura 2.2 *Generador de la ley de comportamiento*

A continuación se crean las piezas. Para la chapa metálica, se selecciona la opción elasto-plástico en la ventana principal del *pre-processor*, y se le establece el material previamente creado.

Para las geometrías, se seleccionará la opción *Geo Primitive*, y se introducirán los datos en mm en la ventada subsiguiente. Nótese que el programa tiene que estar configurado en SI en la ventana de *Simulation Controls*.

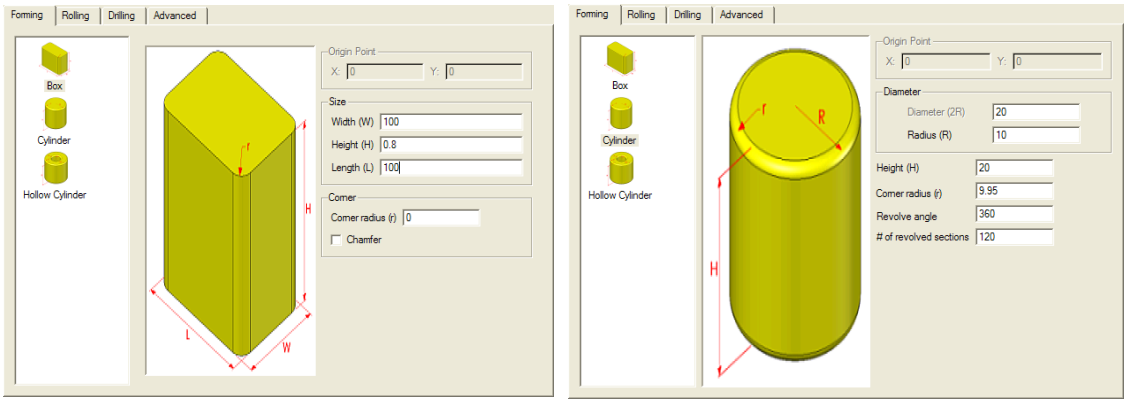

Figura 2.3 *Geometrías de la chapa y el punzón*

Una vez generadas las piezas, hay que ajustar las posiciones relativas de las piezas con la ventana *Object Positioning* en la barra principal para ubicarlas correctamente.

A continuación se creará la malla de la chapa. Para ello se establecerán 150000 elementos, obteniendo finalmente en torno a 50000 (se comprobó que el generador de malla automático reduce los elementos totales a 1/3). Dada la geometría final de la chapa, es necesario refinar la malla en algunas zonas. Para ello, en la pestaña *Detailed Settings*, se establecerá el valor máximo para la opción *Mesh Density Windows* en la pestaña *Weighting Factors*.

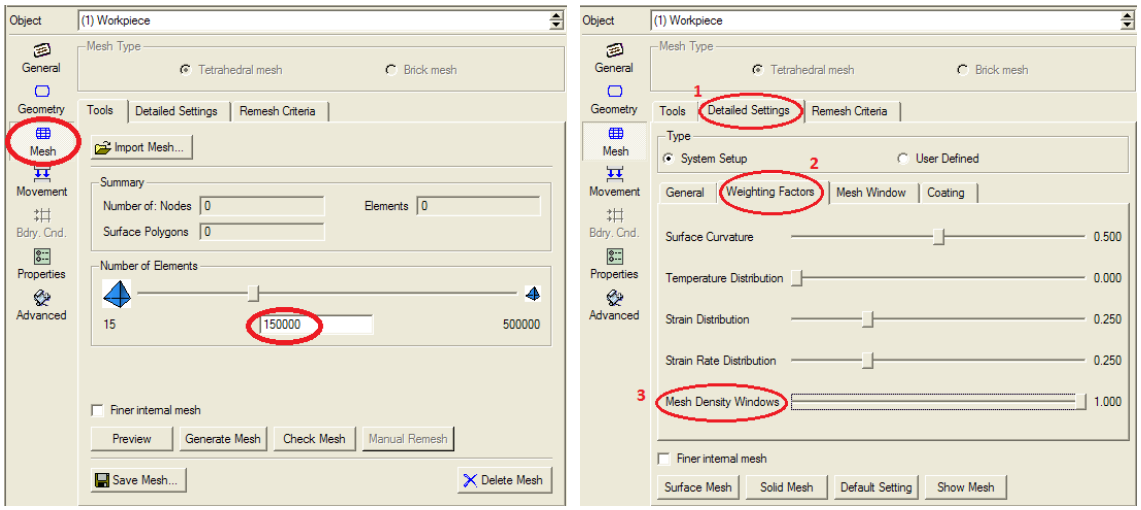

Figura 2.4 *Ventana de mallado de la chapa*

Una vez hecho esto, se crearán dos ventanas de mallado: la interna tendrá un size ratio de 0.12 (al ser la zona más deformada, necesita una malla más fina) y la externa con un ratio de 0.25. Estos valores han demostrado dar resultados aceptables sin grandes tiempos de computación.

Una vez se ha generado la malla, DEFORM™-3D puede dar un fallo en el que las ventanas de mallado no aparecen, siendo una malla uniforme. La solución a esto es sencilla, una vez finalizado el modelo, dejar avanzar el programa unos pasos y remallar manualmente (dado que las ventanas de mallado ya están establecidas, bastará con hacer click en la opción *Generate Mesh*).

Como se ha comentado previamente, a veces en la simulación la malla estaba demasiado distorsionada, generando problemas de *folding*, haciendo necesario parar la simulación y remallar manualmente de nuevo. En esos casos, el nuevo punto de comienzo se estableció en un paso previo a la aparición del mencionado fallo.

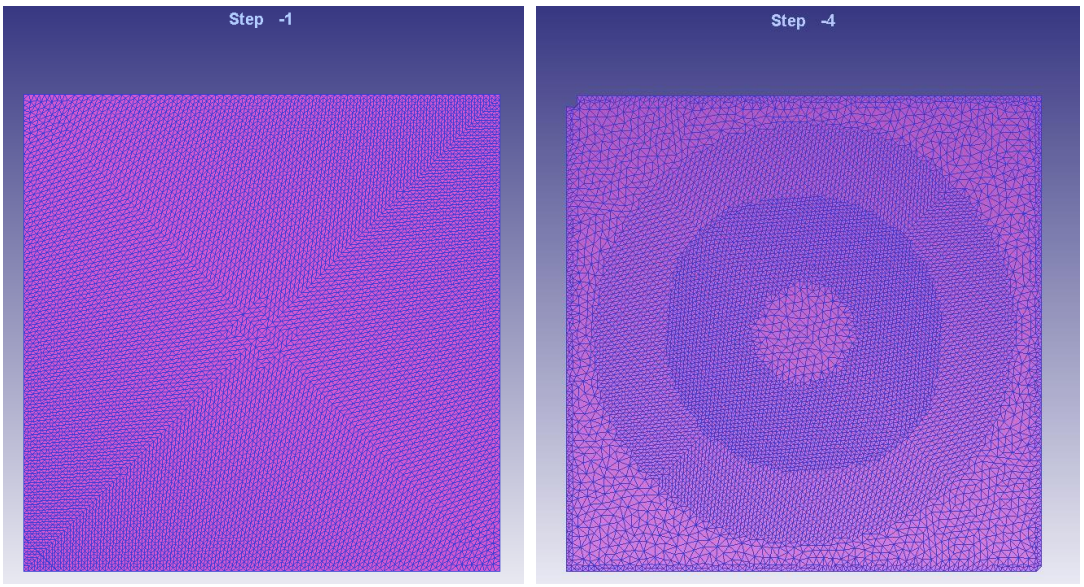

Figura 2.5 *Problema con el mallado (izda) y malla final (dcha)*

Con la malla creada, se pueden establecer las condiciones de contorno en la chapa. Este modelo no presenta b*lank holder* debido a que a partir de cierta profundidad generaba problemas de contacto, introduciéndose la chapa en el *blank holder* en invalidando los resultados a partir de ese punto. Por tanto, una condición de contorno sustituta es necesaria.

La solución de compromiso a la que se llegó para adaptarse a las condiciones experimentales, fue empotrar los extremos de la chapa, y colocar una condición extra en la que se imponía el nulo desplazamiento vertical de los nodos externos a una circunferencia de 42 mm (este valor se usó para ajustar el *blank holder* experimental, que tenía un radio interno de 40 mm y un borde redondeado de 2 mm).

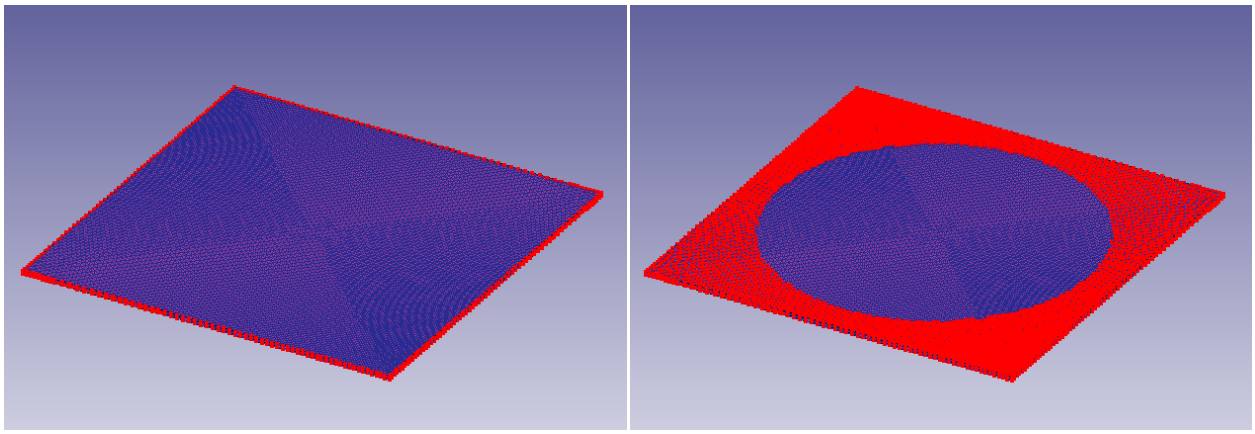

Figure 2.6 *Condiciones de contorno en direcciones x e y* (izda.) *y en dirección z* (dcha.)

Para el movimiento de la herramienta, se genera una nube de puntos mediante PHYTON™ que describen la trayectoria real realizada por la herramienta, dejando todos los parámetros igual que en la experimentación (*feed rate* de 3000mm/min y *step down* de 0.5mm) excepto la rotación de la herramienta sobre sí misma, que no se incluyó en el modelo.

Una vez se tiene la nube de puntos, se selecciona la herramienta en el árbol de piezas, y en la pestaña *Movement* se elige la opción *Path*. Como los datos que tenemos es la trayectoria y la velocidad de avance del punzón, se elige la opción *Profile+feed rate*, y se introducen los puntos en la ventana subsiguiente, que aparece al hacer click en *Define function*.

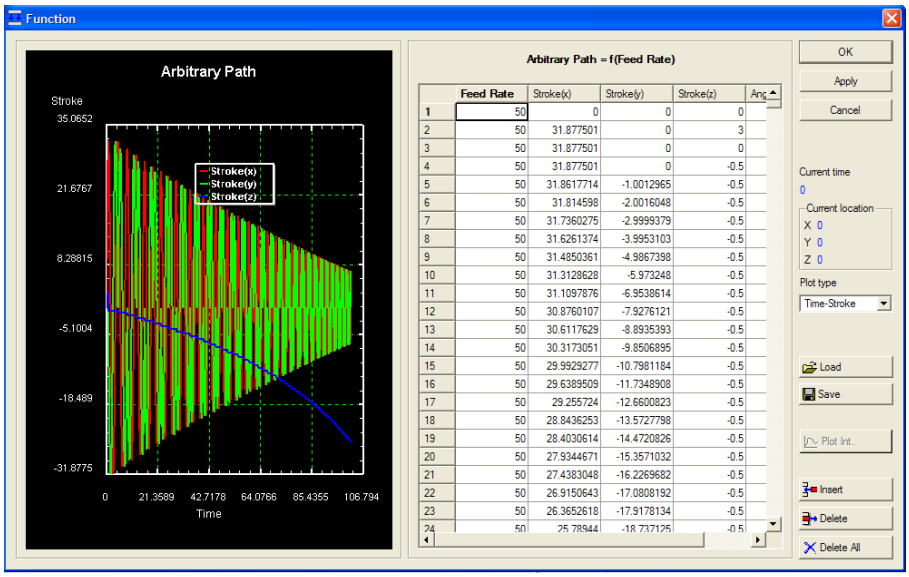

Figura 2.7 *Nube de puntos de la trayectoria*

A continuación se selecciona el *Inter-Object* para establecer la relación entre las piezas, siendo la pieza maestra la herramienta y la esclava la chapa. Con esto seleccionado, queda por establecer la fricción con un valor de 0.01 de Coulomb y generar la relación.

Finalmente, se establecen el número de pasos necesarios en la ventana de *Simulation Controls*, calculados dividiendo el tiempo real entre el *step increment control* (que se estableció en 0.005 s/paso) obteniendo unos 22000 pasos.

Antes de iniciar la simulación, se tiene que generar una base de datos, que requiere ser comprobada primero, ambas opciones ubicadas en la ventana que se abre al clickar en *Database Generation*:

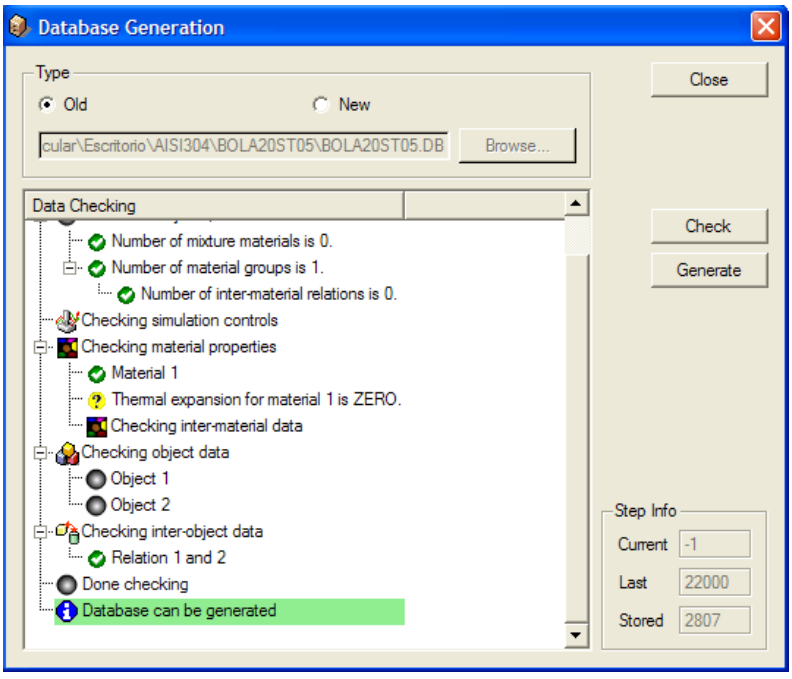

Figura 2.8 *Generación de la base de datos*

Con la base de datos creada, basta con cerrar el *pre-processor* e iniciar la simulación haciendo click en el botón *run*.en la ventana principal de DEFORM™-3D.

A continuación se exponen brevemente los resultados en términos de deformaciones principales obtenidos para la herramienta de 20 mm:

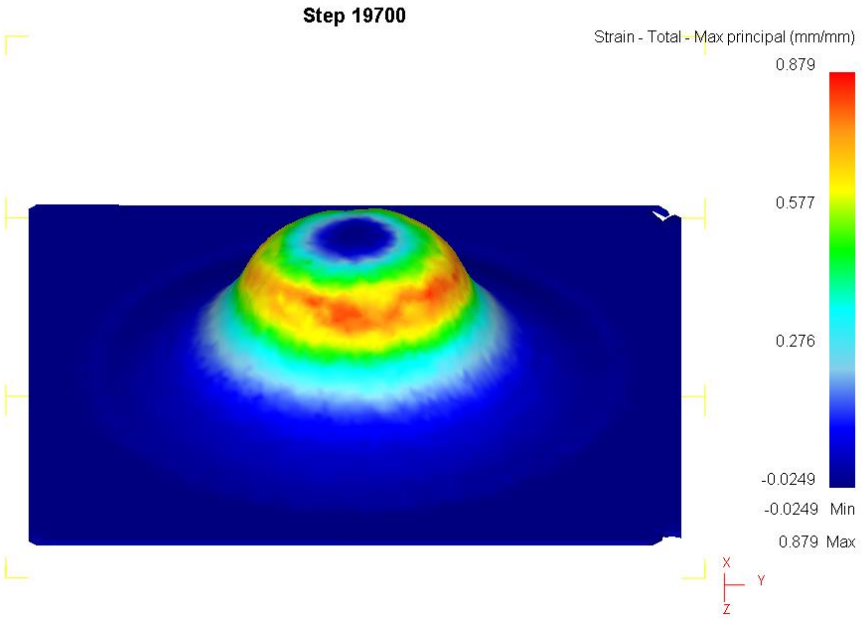

Figura 2.9 *Distribución de la deformación principal ε_1 en la cara contraria a la acción del punzón de 20 mm de diámetro en una placa de AISI304-H111 conformada por SPIF*

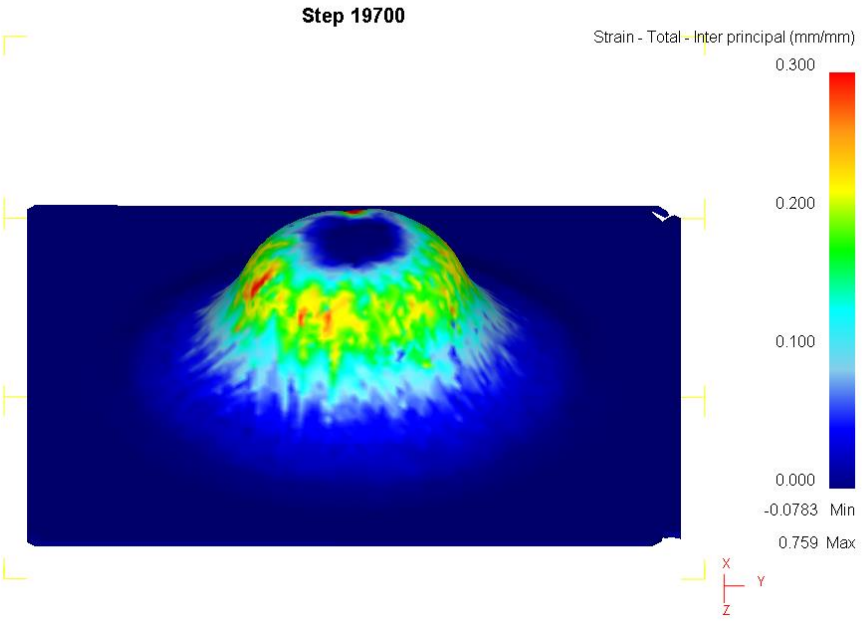

Figura 2.10 *Distribución de la deformación principal ε_2 en la cara contraria a la acción del punzón de 20 mm de diámetro en una placa de AISI304-H111 conformada por SPIF*

Estos resultados corroboran lo obtenido experimentalmente, estando los valores de la deformación principal ε_1 dentro del margen obtenido experimentalmente, habiendo zonas con valores en torno a 0.9 (coloreadas en rojo); mientras que para la deformación principal ε_2 los valores suelen estar en torno a 0.15-0.2, con zonas puntuales en torno 0.3.

Conviene mencionar que hay una zona en la que los valores de ε_2 aumentan hasta 0.8, en el área donde la herramienta realiza el *step down*. Esto no se corresponde con los resultados experimentales, y es probablemente debido a errores numéricos provocados en cada bajada. Como la experimentación muestra que la fractura no ocurre en esa zona, se obviarán los resultados de la zona de bajada de la herramienta.

Por tanto, a la vista de los resultados, se concluye que el modelo es válido, siendo capaz de predecir aceptablemente los flujos de material, y los resultados en deformaciones y tensiones en toda la geometría, exceptuando la zona de bajada de la herramienta previamente mencionada.

3 CONCLUSIONES

En este proyecto se ha creado un modelo de elementos finitos en DEFORM™-3D, para chapas metálicas de acero AISI304-H111 de 0.8 mm de espesor, para analizar el estado de deformaciones a lo largo del proceso. Después de comparar los resultados de la simulación con los experimentales obtenidos por Centeno et al (2014), se ha probado que la simulación se ajusta a la experimentación, permitiendo validar el modelo numérico.

Debido a los grandes tiempos de computación, varias hipótesis simplificadoras se aplicaron al modelo, como considerar el material isótropo, y el empotramiento de los extremos de la placa. También vale la pena mencionar, aunque no fuese para reducir tiempo de computación, la condición de contorno vertical que reemplaza el *blank holder* para solucionar los problemas numéricos comentados.

Esas simplificaciones afectan a las pequeñas diferencias entre los resultados numéricos y los experimentales, pero se hicieron de manera que los resultados numéricos seguían a los experimentales, a la vez que reducían tiempo de computación.

Así, las simulaciones se completaron siguiendo los mismos parámetros que los análisis experimentales. Se llevaron a cabo con herramientas de 20 mm y 10 mm de diámetro, y un *step down* de 0.5 mm. Por tanto, no se simularon todos los tests experimentales (ya que también se probó un *step down* de 0.2mm en la experimentación), pero dado que los resultados para cada *step down* demostraron ser muy similares entre sí, no se ha considerado necesario. En ambas simulaciones, las deformaciones principales a la profundidad de fallo real fueron muy similares a las experimentales.

Además, una vez acabadas y analizadas las simulaciones, se creó un manual paso a paso para mostrar fácilmente cómo modelar los procesos de conformado incremental llevados a cabo en este proyecto con DEFORM™-3D.